Charles University in Prague
Faculty of Mathematics and Physics

Stockholm University
Faculty of Science

DOCTORAL THESIS

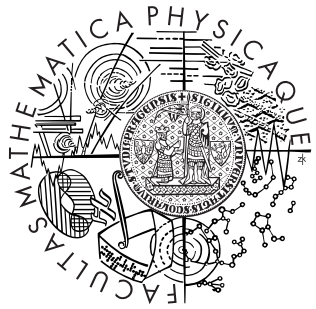

Stockholm University

Mária Šoltésová

Fast Dynamic Processes in Solution Studied by NMR Spectroscopy

Department of Low Temperature Physics

Department of Materials and Environmental Chemistry

Supervisors of the doctoral thesis: doc. RNDr. Jan Lang, Ph.D.
prof. Jozef Kowalewski

Study programme: Physics

Specialization: Biophysics, Chemical and Macromolecular Physics

Prague 2013

Doctoral Thesis 2013

This dissertation work was realized within the framework of the "Agreement of Joint Responsibility for PhD Education and Examination" between Stockholm University and Charles University in Prague.

Faculty Opponent:
prof. Gyula Batta
Department of Organic Chemistry
University of Debrecen, Hungary

Evaluation committee:
prof. Lena Mäler
Department of Biochemistry and Biophysics
Stockholm University, Sweden

prof. István Furó
School of Chemical Science and Engineering
Royal Institute of Technology, Sweden

prof. Jaromír Plášek
Institute of Physics
Charles University in Prague, Czech Republic

prof. Elke Schweda
Department of Physics, Chemistry and Biology
Linköping University, Sweden

prof. Helena Štěpánková
Department of Low Temperature Physics
Charles University in Prague, Czech Republic

Cover: Molecules of polysaccharide, ethanol, cryptophane-C, and trisaccharide and their spectra.

ISBN 978-91-7447-741-2

Printed in Sweden by US-AB, Stockholm 2013

Distributor: Department of Materials and Environmental Chemistry, Stockholm University

Venované mojej rodine

Nothing in life is to be feared. It is only to be understood.

Marie Curie-Skłodowska

I declare that I carried out this doctoral thesis independently, and only with the cited sources, literature and other professional sources.

I understand that my work relates to the rights and obligations under the Act No. 121/2000 Coll., the Copyright Act, as amended, in particular the fact that the Charles University in Prague has the right to conclude a license agreement on the use of this work as a school work pursuant to Section 60 paragraph 1 of the Copyright Act.

In Stockholm, 21st August 2013 Mária Šoltésová

Abstract

Title: Fast Dynamic Processes in Solution Studied by NMR Spectroscopy

Author: Mária Šoltésová

Department: Department of low temperature physics, Charles University in Prague, and Department of Materials and Environmental Chemistry, Stockholm University

Supervisor: doc. RNDr. Jan Lang, Ph.D., Department of low temperature physics, Charles University in Prague, and Prof. Jozef Kowalewski, Department of Materials and Environmental Chemistry, Stockholm University

Abstract: Nuclear magnetic resonance (NMR) spectroscopy is capable to deliver a detailed information about the dynamics on molecular level in a wide range of time scales, especially if accompanied by suitably chosen theoretical tools. In this work, we employed a set of high-resolution NMR techniques to investigate dynamics processes in several weakly interacting molecular systems in solution.

Van der Waals interactions play an important role in inclusion complexes of cryptophane-C with chloroform or dichloromethane. The complex formation was thoroughly investigated by means of ^{1}H and ^{13}C NMR experiments along with the quantum-chemical density functional theory (DFT) calculations. We characterized kinetics, thermodynamics, as well as fine details of structural rearrangements of the complex formation.

Internal dynamics of oligo- and polysaccharides presents a considerable challenge due to possible coupling of internal and global molecular motions. Two small oligosaccharides were investigated as test cases for a newly developed integrated approach for interpreting the dynamics of the molecules with non-trivial internal flexibility. The approach comprised advanced theoretical tools, including stochastic modeling, molecular dynamics (MD) simulations, and hydrodynamic simulations.

A biologically important bacterial O-antigenic polysaccharide from *E. Coli* O91 was addressed employing selective isotope labeling and multiple-field ^{13}C relaxation experiments. The complex dynamics of the polysaccharide is characterized by the conformational motion of the exocyclic groups of the sugars, superimposed to the breathing motion of the polymeric chain.

Hydrogen bonding is another major non-covalent interaction. Dilute solutions of ethanol were chosen as a model of liquid systems containing extensive hydrogen-bonded networks. We developed a new methodology consisting of NMR diffusion measurements, DFT calculations, and hydrodynamic modeling and utilized it to determine average size of the molecular clusters of ethanol at given conditions.

Keywords: Nuclear magnetic resonance, Dynamics, Ethanol, Cryptophanes, Saccharides

Abstrakt

Název práce: Rychlé dynamické procesy v roztoku studované pomocí NMR

Autor: Mária Šoltésová

Katedra: Katedra fyziky nízkých teplot, Univerzita Karlova v Praze a Department of Materials and Environmental Chemistry, Stockholm University

Vedoucí disertační práce: doc. RNDr. Jan Lang, Ph.D., Katedra fyziky nízkých teplot, Univerzita Karlova v Praze a prof. Jozef Kowalewski, Department of Materials and Environmental Chemistry, Stockholm University

Abstrakt: Nukleární magnetická rezonance (NMR) dokáže poskytnout detailní informace o dynamice na molekulární úrovni v širokém oboru časových škál, zejména pokud je doplněna vhodnými teoretickými nástroji. V této práci byla použita sada technik NMR spektroskopie vysokého rozlišení pro výzkum dynamických procesů slabě interagujících molekulárních struktur v roztoku.

Van der Waalsovy interakce hrají důležitou roli v inkluzních komplexech kryptofanu-C s chloroformem nebo dichlormethanem. Tvorba komplexu byla podrobně zkoumána za použití ^{1}H a ^{13}C NMR experimentů spolu s kvantově-chemickými výpočty. Byla charakterizována kinetika, termodynamika, jakož i detaily strukturních změn při tvorbě komplexu.

Vnitřní dynamika oligo- a polysacharidů představuje velkou výzvu kvůli možnému provázání lokálního a globálního molekulárního pohybu. Dva modelové oligosacharidy byly použity pro testování nově vyvinuté integrované metody pro popis dynamiky molekul s netriviální vnitřní flexibilitou. Tato metoda spojuje pokročilé teoretické výpočty včetně stochastického modelování, simulací molekulové dynamiky a hydrodynamiky.

Antigenní bakteriální polysacharid z *E. Coli* O91, důležitý z biologického hlediska, byl studován za pomoci selektivního izotopového značení a NMR relaxačních experimentů ve více magnetických polích. Komplexní dynamika polysacharidu je charakterizována konformačními změnami exocyklických skupin cukerných reziduí a omezenou interní flexibilitou polymerního řetězce.

Vodíkové vazby jsou další z důležitých nekovalentních interakcí. Zředěné roztoky ethanolu byly vybrány jako model kapalného systému obsahujícího rozsáhlou síť vodíkových vazeb. Vyvinuli jsme novou metodologii, složenou z NMR difúzních měření, kvantově-chemických výpočtů a hydrodynamického modelování a aplikovali ji pro zjištění průměrné velikosti molekulových klastrů ethanolu za specifických podmínek.

Klíčová slova: Nukleární magnetická rezonance, dynamika, ethanol, kryptofan, sacharidy

List of Papers

The following papers, referred to in the text by their Roman numerals, are included in this thesis.

PAPER I: **NMR Investigation of Guest-Host Complex between Chloroform and Cryptophane C**
Z. Takacs, M. Šoltésová, D. Kotsyubynskyy, J. Kowalewski, J. Lang, T. Brotin, and J. P. Dutasta
Magn. Reson. Chem., **48**, 623–629 (2010).

My contribution: Taking a major part at acquiring of the NMR experimental data including their analysis, major contribution to interpretation of the data and discussions of the results.

PAPER II: **Host-Guest Complexes between Cryptophane-C and Chloromethanes Revisited**
Z. Takacs, M. Šoltésová, J. Kowalewski, J. Lang, T. Brotin, and J.-P. Dutasta
Magn. Reson. Chem., **51**, 19–31 (2013).

My contribution: Taking part at acquiring of the NMR experimental data, contributing to interpretation of the data and discussions of the results.

PAPER III: **Stochastic Modeling of Flexible Biomolecules Applied to NMR Relaxation. 2. Interpretation of Complex Dynamics in Linear Oligosaccharides**
D. Kotsyubynskyy, M. Zerbetto, M. Šoltésová, O. Engström, R. Pendrill, J. Kowalewski, G. Widmalm, and A. Polimeno,
J. Phys. Chem. B, **116**, 14541–14555 (2012).

My contribution: Acquiring of the NMR experimental data for the trisaccharide and their analysis, performing the interpretation of the NMR data using the DCM model.

PAPER IV: **Dynamics of Exocylic Groups in the *Escherichia coli* O91 O-Antigen Polysaccharide in Solution Studied by Carbon-13 NMR Relaxation**
M. Šoltésová, J. Kowalewski, and G. Widmalm
J. Biomol. NMR, *Accepted for publication*

My contribution: Acquiring of the NMR experimental data including their analysis, performing the interpretation of the data using various motional models. Major contribution to discussions of the results and preparation of the manuscript and figures.

PAPER V: **Determination of Size of Molecular Clusters of Ethanol by Means of Diffusion NMR and Hydrodynamic Calculations**
M. Šoltésová, M. Peksa, L. Benda, J. Czernek, and J. Lang,
in manuscript

My contribution: Sample preparation, acquiring of the NMR experimental data including their analysis, performing hydrodynamic simulations, interpretation of the data. Major contribution to discussions of the results and preparation of the manuscript and figures.

Contents

List of Figures

List of Tables

1. Introduction

Investigation of biomolecules such as proteins, carbohydrates, nucleic acids, and possibly their complexes, is undoubtedly important, and therefore a topic of extensive interest in the chemistry- and biology-related research fields. The systems of biological interest are often large and complicated and their investigation represents a challenge at both experimental and theoretical levels.

Not only the structure of these systems but also their interactions and dynamics are of great importance in description of their biological function. The motions of the molecules are strongly interrelated with their interactions and thus their biological functions. To fully understand the phenomena ongoing in the complex systems, it is sometimes essential to abandon the complicated cases and turn to simpler, yet realistic, model systems.

An example of a phenomenon that is very complex and plays significant role in the biological systems is hydrogen bonding. A better understanding can be achieved by means of studying systems composed of small organic molecules. The relative simplicity of such systems can provide an invaluable insight into the important features of the hydrogen-bonded complexes.

Utilization of hydrogen bonding and other non-covalent interactions gave rise to the rich field of supramolecular chemistry with many promising applications. Cryptophane molecules, with their ability to form supramolecular complexes, can serve as model systems for molecular recognition or biological receptors.

Other instances are small or medium-sized molecules that can serve as test cases for theoretical models that are designed to describe complex molecular dynamics.

The studies included in this work incorporate at the first sight rather diverse systems, from small ethanol molecules, through cryptophanes and oligosaccharides, to a somewhat larger polysaccharide, all described in detail in Chapter 2. The common attribute, which makes these systems and associated phenomena interesting to explore, is their dynamics, to a large extend affected by weak molecular interactions.

Nuclear magnetic resonance (NMR) spectroscopy is one of the most important spectroscopic techniques which can provide an informative insight into the motional properties of various systems. Nowadays, the researchers can profit from the fast developing methodology and improving sensitivity of NMR

that opens the possibility to employ a wide range of experiments. The basic principles and methods of NMR spectroscopy are explained in Chapter 3.

The ability to probe the molecular motion over a wide range of timescales, ranging from picoseconds to tens of seconds or even longer, is one of the most important and useful features of NMR. It is obvious that molecules in solution are not rigid objects but undergo a full range of imaginable motions. Starting from the fastest, we can mention bond vibrations and librations (10^{-12} s or faster) and local rotation of molecular groups (10^{-12} s or slower), and continue with slower motions corresponding to molecular flexibility of large molecular "chains" and molecular rotations (10^{-12}–10^{-9} s). The list can be closed with motion that can be as slow as seconds, such as breaking and reforming of molecular bonds (10^{-9} s up to seconds). A motion on a macroscopic scale, such as translational diffusion, is also included in the list of phenomena observable by NMR. Figure 1.1 summarizes the timescales of various molecular motions and the possibilities to detect them by NMR methods within the scope of this work.

It is clear that to cover such a large variety of timescales, the principle of the methods for their observation have to be different. Chemical reactions or other processes, where the studied species are changing their chemical environment, are commonly denoted as chemical exchange, and can occur on timescales from microseconds up to seconds or even longer. Such processes can be studied by exchange methods described in Section 3.4. Examples of systems undergoing chemical exchange are host-guest complexes of cryptophanes, discussed in Papers I and II.

For the molecular motions that occur on the picoseconds to nanoseconds

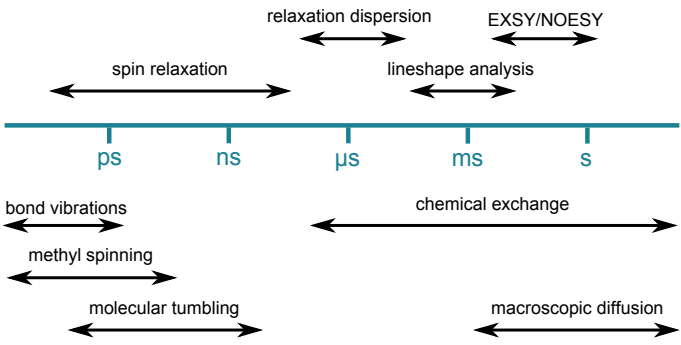

Figure 1.1: Schematic representation of the approximate timescales of the molecular motions (lower part) and their possibility to detect them by various NMR experimental techniques (upper part).

timescales, NMR spin relaxation has proven to be especially sensitive technique. Theoretical and experimental aspects of the spin relaxation are described in Section 3.5. An example of dynamics which can be studied using NMR relaxation is the internal motion of oligosaccharides and polysaccharides, studied in Papers III and IV.

Finally, the translational diffusion, described in Section 3.3, can be utilized to address the hydrogen bonding phenomenon, as shown in Paper V. Here, NMR diffusion measurements were used to investigate the hydrogen-bonded clusters of ethanol.

2. Studied systems

2.1 Cryptophanes and host-guest complexes

Cryptophanes are medium-sized molecules known for their ability of binding small molecular guests inside their cavity. Since their first synthesis and characterization by Collet and coworkers in 1980s [1–5], they have received extensive attention in both theoretical and experimental studies. Several reviews discussing the chemistry of cryptophanes have been published, the most recent by Brotin and Dutasta [6].

Cryptophanes consist of two cyclotribenzylene (CTB) units (the caps), connected by three aliphatic linkers of the -O-$(CH_2)_n$-O- type. There is a large variability of cryptophanes in terms of different substituents on the caps or modifications of the linkers. The connection of the linkers to the caps defines the *syn* or *anti* isomer, as schematically depicted in Figure 2.1. Among the cryptophanes studied recently in our laboratory we can mention cryptophane-A, cryptophane-C, and cryptophane-D with $n = 2$, and cryptophane-E with $n = 3$, depicted in Figure 2.2.

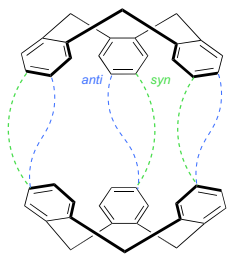

Figure 2.1: *Anti* and *syn* isomer a cryptophane: two possible ways of connection of the aliphatic -O-$(CH_2)_n$-O- linkers to the CTB caps.

Cryptophane-A is an *anti* isomer, having two identical caps, both carrying methoxy substituents on each phenyl group. Cryptophanes C and D have methoxy groups only on one of the caps. They are diastereoisomers – cryptophane-C is the *anti* isomer and cryptophane-D is the *syn* isomer.

An interesting issue is the conformation of the linkers, since it affects the

symmetry properties of the cryptophane molecule as well as the size of the cavity. The linkers of cryptophanes C and D can be found in either *gauche* or *trans* conformation. Moreover, there are two types of *trans* conformers denoted T_1 and T_2, each having the -O-CH_2-CH_2-O- dihedral angle of 180°, but differing in the relative position of the CH_2 groups with respect to the oxygens. In the case of *gauche* conformation, the -O-CH_2-CH_2-O- dihedral angle is 60° (G_-) or $-60°$ (G_+). In analogy with the *trans* case, both conformations can additionally differ in the relative position of the CH_2 groups with respect to the oxygens. This gives four possibilities for *gauche* conformers, denoted $G_{\pm 1}$ and $G_{\pm 2}$.

The conformation of the cryptophane molecule is defined by the conformation of each of its three linkers (e.g. $T_1T_1T_1$). Even if degeneracies due to the symmetry of the molecule are considered, the number of possible conformers is large .

Cryptophanes possess a hydrophobic cavity, in which they can encapsulate a small organic guest molecule. Among the most favorable guests are halomethanes, for example chloroform ($CHCl_3$), dichloromethane (CH_2Cl_2), chloromethane, bromomethane, iodomethane and others. The complex is held together by van der Waals interactions.

The focus of this work was on cryptophane-C and its complexation with chloroform and dichloromethane, investigated in Papers I and II.

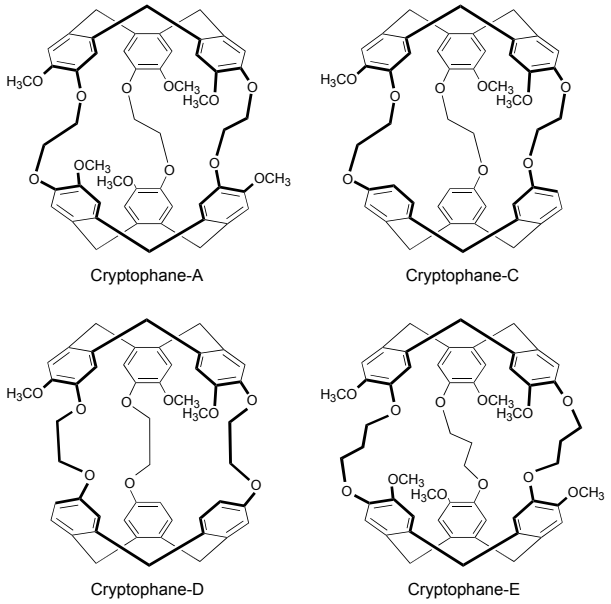

Figure 2.2: Examples of cryptophanes

2.2 A trisaccharide as an example of complex internal dynamics

A linear trisaccharide, composed of three mannose residues α-D-Man*p*-(1→2)-α-D-Man*p*-(1→6)-α-D-[6-^{13}C]-Man*p*-OMe, was subject of the study reported in Paper III. This relatively simple molecule is an interesting model system for both experimental and theoretical investigation due to its complex dynamics. The internal flexibility is described by the rotation around the glycosidic linkages, the two important torsions are defined by angles denoted ω and ψ_2 in Figure 2.3.

As it was anticipated [7], the internal motion is coupled to the overall tumbling of the molecule due to the similar timescales, thus interpretation of the dynamics using common methods becomes particularly difficult. For this reason, the trisaccharide became an interesting study case for testing an integrated theoretical approach designed to deal with dynamics of molecules described as a flexible chain, i.e. consisting of rigid units linked by joints around which torsional motion is possible.

Paper III describes the performance of the developed approach for interpretation of NMR relaxation data of the trisaccharide and a pentasaccharide.

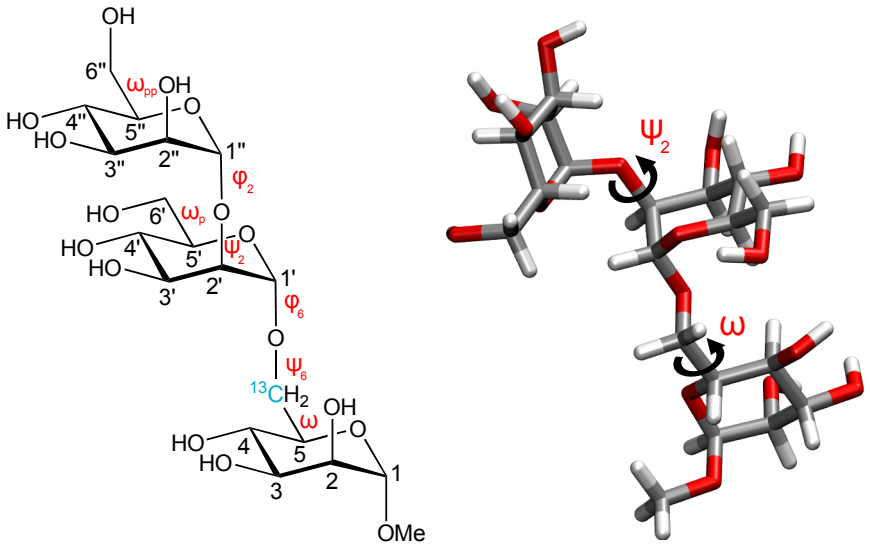

Figure 2.3: Trisaccharide, a schematic representation (left) and a stick model (right). The relevant torsion angles ω and ψ_2 are highlighted.

2.3 *Escherichia coli* O-antigenic polysaccharides

Escherichia coli is usually a non-pathogenic facultative anaerobe present in human colonic flora. However, several *E. coli* strains have acquired specific virulent factors and may cause variety of infections in humans and animals. Among the *E. coli* causing intestinal diseases, there are six well-described pathotypes. Among them are the enterohemorrhagic bacteria, where *Escherichia coli* O91 belongs. The typing of the bacteria is based on their O (somatic), H (flagellar) and K (capsular) surface polysaccharide antigens. More than 180 O, 60 H and 80 K antigens have been proposed up to date. Each O-antigen defines a serogroup, a specific combination of O and H antigens defines the serotype of the bacteria. Each pathotype may comprise several serogroups and one serogroup may belong to several pathotypes and even to non-pathogenic bacteria. The structures of O-antigenic polysaccharides are listed in the database *E. coli* (ECODAB) [8].

The antigenic polysaccharides are a part of the lipopolysaccharides (LPS), also known as endotoxins, which are anchored to the outer membrane of the Gram-negative bacterium. The LPS consists of three parts: the toxic component called *lipid A*; the *core sugar*, or core region, consisting of inner and outer part; and finally the O-antigen polysaccharide (Figure 2.4). The O-antigens of *E. coli* usually consist of 10–25 repeating units containing 2–7 sugar residues.

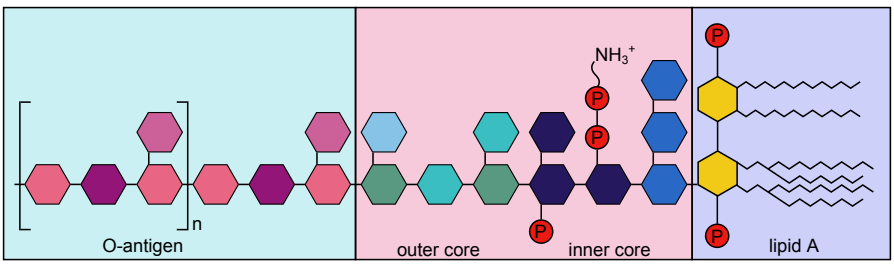

Figure 2.4: Schematic representation of the *E. coli* lipopolysaccharide. The O-antigenic chain consists of $n \approx$10–25 repeating units of 2–7 sugar residues per unit. The composition of the individual parts may vary.

For the determination of the O-polysaccharides, the LPS are extracted from the cultivated bacteria isolates and the O-polysaccharide is released from the lipid A part by treatment with dilute acid and purified by gel-permeation chromatography. NMR spectroscopy, accompanied by hydrolysis and subsequent gas-liquid chromatography/mass spectroscopy (GLC-MS) and high performance liquid chromatography (HPLC), is often the method of choice for structural investigation of the separated polysaccharide.

NMR spectroscopy can be also helpful in determination of the biosynthetic pathway of the LPS O-antigen. In *Escherichia coli*, two distinct mechanisms of the synthesis of the O-antigenic polysaccharide have been described. In some bacteria, the polymerization occurs via the transfer of the growing chain to a newly synthesized repeating unit on undecaprenolphosphate, a membrane bound carrier, termed *Wzy-polymerase-dependent* pathway. In another described pathway, the polysaccharide is formed at the cytoplasmatic face of the inner cell membrane by the transfer of glycosyl residues to the non-reducing end and subsequently transported to the periplasmatic face, called *ABC-transporter-dependent* pathway [9–11].

2.3.1 *E. Coli* O91 O-antigenic polysaccharide

The species of our interest was the O-antigenic polysaccharide from the enterohemorrhagic *E. coli* O91. The structural and biosynthetic study was performed by Kjellberg *et al.* [12] on the ^{13}C-enriched sample isolated from bacteria grown on uniformly labeled D-glucose. It was shown that the *E. Coli* O91 O-antigen is composed of a pentasaccharide repeating unit, consisting of 5 sugar residues denoted **A**–**E**, each of which is a hexopyranosyl entity containing six carbons. The amino sugars **C** and **D** are *N*-acetylated, residue **B** carries a glycinyl group and residue **E** has an (R)-3-hydroxybutyryl group as a substituent. The chemical structure of the repeating unit is listed in Table 2.1 and represented in Figure 2.5.

Table 2.1: Structures of the biological repeating unit of the *E. coli* O91 O-antigen.

residue	sugar
E	→4)-α-D-Qui*p*-3-*N*-[(*R*)-3-hydroxybutyramido]-(1→
A	→4)-β-D-Gal*p*-(1→
D	→4)-β-D-Glc*p*NAc-(1→
B	→4)-β-D-Glc*p*A-6-N-Gly-(1→
C	→3)β-D-Glc*p*NAc-(1→

Additional cultures with specifically labeled D-[1-^{13}C]glucose and D-[6-^{13}C]glucose were grown, resulting in the labeling at, *inter alia*, anomeric carbons (C1 position) and exocyclic groups (C6 position), depicted in Figure 2.5. The NMR experiments performed on these samples revealed the direct incorporation of the enriched glucose in the polysaccharide chain.

The carbon-13 relaxation study on the site-specifically labeled O-antigenic polysaccharide resulting from the D-[1-^{13}C]glucose growth was later performed

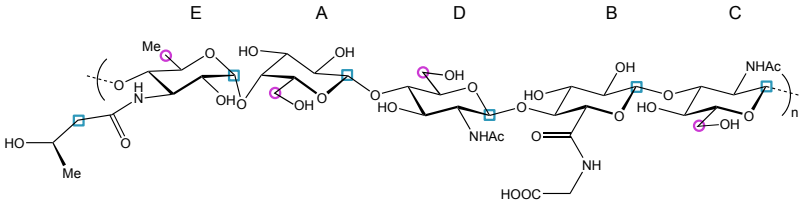

Figure 2.5: The structure of the biological repeating unit of *E. coli* O91 O-antigenic polysaccharide. The specifically labeled sites resulting from growth on D-[1-^{13}C]glucose (turquoise squares) and D-[6-^{13}C]glucose (magenta circles) are shown.

by Lycknert and Widmalm [13]. The biological repeating unit was shown to be defined as **E**-**A**-**D**-**B**-**C** and the polysaccharide was estimated to have $n \approx 10$ repeating units. The analysis of the relaxation data revealed complex dynamics behavior, where the internal motion of the sugar rings varied with their position in the repeating unit.

The growth on D-[6-^{13}C]glucose led to the second selective labeling scheme, where the exocyclic groups of the sugar residues (C6 carbons) received ^{13}C isotopes. Investigation of the dynamics of the O-antigenic polysaccharide with this labeling scheme was a subject of the study presented in Paper IV.

2.4 Hydrogen-bonded clusters of ethanol

2.4.1 Hydrogen bonds

The hydrogen bond is one of the most important non-covalent interactions. Although the hydrogen-bonding phenomenon was discovered almost 100 years ago, it is still a topic of extensive scientific research. The reason for the unceasing interest lies in the importance of hydrogen bonding for structural, functional and dynamic properties of a vast number of systems, ranging through all branches of chemistry.

In terms of modern concepts, the hydrogen bond is understood as a very broad phenomenon [14–17]. There are many different types of hydrogen bonds whose dissociation energies cover more than two orders of magnitude (about 0.2–40 kcal.mol^{-1}) [18; 19]. The precise definition of a hydrogen bond is therefore a problematic issue.

In a "classical" view, the hydrogen bond, symbolized X — H $\cdots$ A, can be defined as an attractive interaction occurring between a strongly polar group $X^{\delta-}$ — $H^{\delta+}$ on one side, and an electronegative atom $A^{\delta-}$ on the other side. The group X — H is called the *proton donor* and contains a hydrogen atom

that plays a fundamental role in the interaction. The moiety A is called the *proton acceptor*. In order to be able to form hydrogen bonds, the X — H group has to be at least slightly polar and A should supply a sterically accessible concentration of negative charge (usually a lone pair of electrons). An example of a hydrogen bond between two molecules of ethanol is depicted in Figure 2.6. Among the important characteristics distinguishing hydrogen bonds from van der Waals interactions is their directionality – a preference of linearity.

Hydrogen bonding is the key to understanding the structure and properties of variety of neat liquids as well as their mixtures. Particularly interesting are those consisting of molecules containing hydroxyl groups, which can create hydrogen bonds where the oxygen acts both as the proton acceptor and donor (O — H···O). This fact allows for complicated hydrogen-bonded networks in water, low-molecular-weight alcohols and other liquids. Moreover, significant cooperative effects are observed in arrays of hydrogen bonds [20–22]. Once a molecule is engaged as a hydrogen donor, it automatically becomes a better acceptor, and *vice versa*.

In Paper V, we have studied the hydrogen bonding in a solution of liquid ethanol in a non-polar solvent. The molecules of ethanol are known to form hydrogen-bonded aggregates, called *molecular clusters*. Ethanol is expected to form less complicated structures than for instance water, where the clusters of hydrogen-bonded molecules can be large and of extensive variety. Nevertheless, ethanol clusters can still consist of a varying number of molecules and have quite diverse possible topologies, details of which are not completely understood. Examples of pentameric cyclic and linear ethanol clusters are depicted in Figure 2.7.

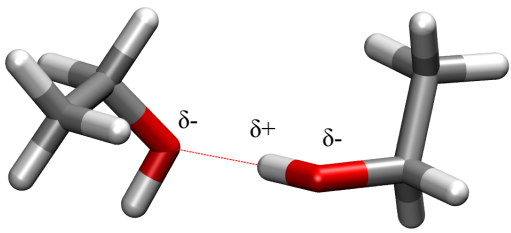

Figure 2.6: Schematic representation of a hydrogen bond between two ethanol molecules.

2.4.2 Hydrogen bonding and NMR

The hydrogen-bonded molecular clusters can be investigated by a variety of experimental methods, including X-ray and neutron diffraction, infrared spectroscopy, Raman spectroscopy, NMR spectroscopy, as well as theoretical approaches. Several works dealing with hydrogen-bond issue employing different approaches are discussed in Paper V.

NMR spectroscopy is a powerful probe of hydrogen bond. The consequences of the hydrogen-bonding phenomenon can be investigated at two stages.

The first one is the direct influence on NMR spectra, where the change in the chemical shift of the hydroxyl protons is attributed to their involvement in hydrogen bonds. This effect was recognized as early as in 1950s [23; 24]. In particular, the length of a hydrogen bond of the type O — H $\cdots$ O is a good qualitative measure of its strength. The increase of the strength of the hydrogen bond leads to shortening of the hydrogen bond and to an elongation of the covalent O — H bond on the other side. Furthermore, a shorter hydrogen bond leads to increased deshielding of the proton involved in the hydrogen bond, and thus to the ^{1}H downfield shift that is correlated with the strength of the hydrogen bond.

The other possibility of probing hydrogen bonds by NMR became feasible with the development of pulsed field gradient NMR techniques. These allow for measuring of the translational diffusion, which is clearly affected by the aggregation of molecules into hydrogen-bonded clusters.

The NMR diffusion measurements together with the DFT calculations and hydrodynamic simulations were our methods of choice for investigation of hydrogen-bonding in ethanol, described in paper V.

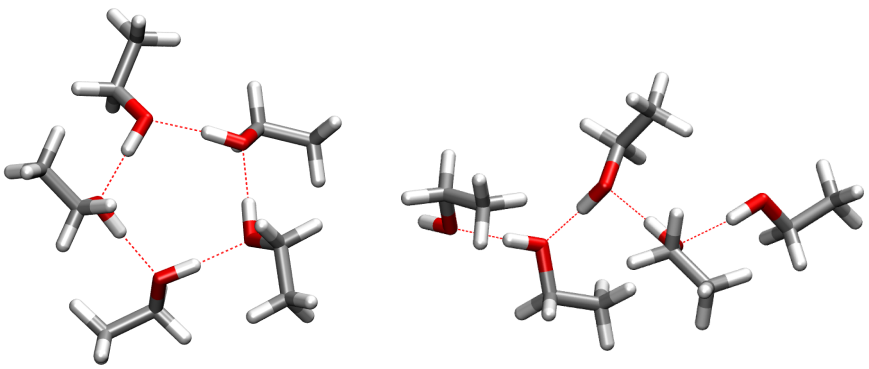

Figure 2.7: Examples of hydrogen-bonded clusters of ethanol: a cyclic pentamer (left) and a linear pentamer (right).

3. Theory and methods

This chapter aims at a brief description of common principles of high-resolution nuclear magnetic resonance with the focus on dynamic processes in solution and their investigation by NMR. Detailed description can be found in several textbooks, for example [25–29].

3.1 Basic principles of NMR

Nuclear magnetic resonance is a phenomenon at which resonating behavior of nuclei with non-zero spin angular momentum $\hat{\boldsymbol{I}}$ (with its components $\hat{I}_x$, $\hat{I}_y$, $\hat{I}_z$ and its spin quantum number I) in external magnetic field is observed. Nuclei with non-zero spin also possess the nuclear magnetic moment $\hat{\boldsymbol{\mu}}$, related to the spin angular momentum of the nucleus as

$$\hat{\boldsymbol{\mu}} = \gamma\hbar\hat{\boldsymbol{I}}, \tag{3.1}$$

where $\hbar$ is the reduced Planck constant and the quantity γ is called the *magnetogyric ratio* or *γ-factor*.

When a nuclear spin is placed into an external magnetic field $\boldsymbol{B}$, the field interacts with the magnetic moment via *Zeeman interaction*, described by the *Zeeman Hamiltonian*

$$\hat{H}_0 = -\hat{\boldsymbol{\mu}} \cdot \boldsymbol{B} = -\gamma\hbar\hat{\boldsymbol{I}} \cdot \boldsymbol{B}. \tag{3.2}$$

A large static magnetic field (tens of Tesla), produced usually by a superconducting coil, is essential in high-resolution NMR. The static field is assumed to be oriented along the laboratory-frame z-axis. In this convention $\boldsymbol{B} = (0,0,B_0)$, which simplifies the Zeeman Hamiltonian in Eq. 3.2 to

$$\hat{H}_0 = -\gamma\hbar\hat{I}_z B_0. \tag{3.3}$$

Solution of the time-independent Schrödinger equation with the Hamiltonian 3.3 gives $2I+1$ eigenvectors $|I,M\rangle$, called also *Zeeman eigenstates*. Zeeman eigenstates are characterized by the spin quantum number I, possessing either integer or half-integer values, and the magnetic quantum number M in the range of $(-I, -I+1, \ldots, I)$.

The corresponding eigenvalues are the energies of the $2I+1$ equidistant energy levels, characterized by the quantum number M

$$E_M = -\gamma\hbar B_0 M. \tag{3.4}$$

The distance ΔE between the levels is $\Delta E = |\gamma|\,\hbar B_0$.

Nuclei with the nuclear spin quantum number $I = 1/2$ in the ground state, referred further as *spin-1/2* nuclei, are of major importance in NMR. Among the most commonly studied are ^{1}H, ^{13}C, ^{15}N, ^{19}F, etc. In this work, the attention is mostly drawn to experiments on ^{1}H and ^{13}C nuclei. The ^{1}H nuclei, sometimes called also "protons", have a γ-factor of $\gamma_H = 267.522 \times 10^{-6}$ rad s^{-1} T^{-1} and their natural abundance is practically 100 %, thus making this isotope easily observable by NMR. The ^{13}C isotopes, also called "carbon-13" nuclei, have the γ-factor about 4-times lower than protons ($\gamma_C = 67.283 \times 10^{-6}$ rad s^{-1} T^{-1}) and their natural abundance is only 1.1 %, resulting in lower sensitivity than ^{1}H nuclei. One way of dealing with the low sensitivity of carbon-13 experiments is using isotopicaly enriched samples (carbon-13 labeling).

Spin-1/2 nuclei have two Zeeman eigenstates, usually denoted $|\alpha\rangle$ and $|\beta\rangle$, defined as

$$|\alpha\rangle = \left|\tfrac{1}{2}, +\tfrac{1}{2}\right\rangle \qquad |\beta\rangle = \left|\tfrac{1}{2}, -\tfrac{1}{2}\right\rangle. \tag{3.5}$$

The spin is not restricted to the $|\alpha\rangle$ or $|\beta\rangle$ state, but may be in a superposition of the two energy eigenstates

$$|\psi\rangle = c_\alpha\,|\alpha\rangle + c_\beta\,|\beta\rangle\,, \tag{3.6}$$

where c_α and c_β are the (normalized) superposition coefficients. In general, the spin state $|\psi\rangle$ is time-depended and it can be shown, by solving the time-dependent Schrödinger equation with the Hamiltonian 3.3, that the spin precesses around the z-axis with the frequency given by

$$\omega_0 = -\gamma B_0. \tag{3.7}$$

The quantity ω_0 is called the *Larmor frequency* and it is proportional to the external magnetic field strength B_0 and the γ-factor of the nucleus.

3.1.1 Radio-frequency field

The important part of the NMR experiment is a time-dependent external magnetic field, oscillating at the frequency ω_{ref}, called the *radio-frequency field*, or *r.f. field*. It is generated by the excitation coil, usually placed perpendicularly to the direction of the static field. The spin thus experiences two fields

– the static field of the magnet $\mathbf{B}_0$ and the many orders of magnitude smaller r.f. field $\mathbf{B}_{RF}$.

The effect of the r.f. field can be described as a perturbation to the static magnetic field by applying a time-dependent perturbation theory. For simplicity, the motion under the influence of the r.f. field is described in a frame rotating around the direction of $\boldsymbol{B}_0$ (laboratory frame z-axis) with the angular frequency ω_{ref}. The detailed derivation of the motion of the nuclear spin in the presence of the r.f. field is to be found for example in books of Levitt [25] or Keeler [26], here we just summarize the results.

It can be shown that, if the radio-frequency field is applied close to the resonance (i.e. $\omega_{ref} \approx \omega_0$), the motion of the single spin-1/2 can be described as a rotation of the angular momentum around the direction of the $\boldsymbol{B}_{RF}$ (which appears static in the rotating frame). The closer is the frequency of the field ω_{ref} to the Larmor frequency ω_0 of the observed nucleus, the larger the influence on the spin. This resonant behavior is the key principle of nuclear magnetic resonance.

In a typical NMR experiment, the r.f. field is applied in short pulses and the response of the system, known as the *free induction decay*, or FID, is recorded and submitted to the Fourier transform to give an NMR spectrum.

In a special case, when the r.f. field is applied in a pulse of frequency ω_{ref} equal to the Larmor frequency ω_0 of the observed nucleus and the radio-frequency coil is placed along the x-axis (so-called x-phase pulse), the r.f. field causes the rotation of the spin around x-axis by the flip angle given as

$$\beta_p = \tau_p \omega_{nut}, \tag{3.8}$$

where τ_p is the duration of the pulse. The quantity ω_{nut} is called the *nutation frequency* and it represents the magnitude of the r.f. field as

$$\omega_{nut} = |\frac{1}{2}\gamma B_{RF}|. \tag{3.9}$$

If, for example, the r.f. field is applied for a certain τ_p, for which the flip angle is 90°, we denote a pulse like that a $\pi/2$-pulse. In the case of $\beta_p = 180°$, we speak of a π-pulse.

3.1.2 Spin density operator

So far we have discussed the properties of a single spin-1/2 in the magnetic field. Here we consider a more realistic situation, in which a large amount of 1/2-spins is present in a sample. A useful description of such case is the *spin density operator* $\hat{\rho}$, which describes the quantum state of the entire collection

of spins. The spin density operator is given as

$$\hat{\rho} = \frac{1}{N}\sum_j |\psi_j\rangle\langle\psi_j|, \tag{3.10}$$

where the index j samples throughout all the N spins present. In case of an ensemble of identical non-interacting spin-1/2 species, where $|\psi\rangle$ is in the form of Eq. 3.6, we can write the matrix elements of the spin density operator, also referred to as the *density matrix*

$$\hat{\rho} = \begin{pmatrix} \rho_{\alpha\alpha} & \rho_{\alpha\beta} \\ \rho_{\beta\alpha} & \rho_{\beta\beta} \end{pmatrix} = \begin{pmatrix} \overline{c_\alpha c_\alpha *} & \overline{c_\alpha c_\beta *} \\ \overline{c_\beta c_\alpha *} & \overline{c_\beta c_\beta *} \end{pmatrix}. \tag{3.11}$$

The diagonal elements $\rho_{\alpha\alpha}$ and $\rho_{\beta\beta}$ are referred to as the *populations* of the states $|\alpha\rangle$ and $|\beta\rangle$. The off-diagonal elements $\rho_{\alpha\beta}$ and $\rho_{\beta\alpha}$ are called the *coherences* between the states $|\alpha\rangle$ and $|\beta\rangle$. One of the advantages of the density operator construct is that the expectation value for an operator $\hat{Q}$ of an arbitrary observable can be expressed as

$$\langle\hat{Q}\rangle = \mathrm{Tr}\left\{\hat{\rho}\hat{Q}\right\}, \tag{3.12}$$

where "Tr" stands for the trace of the operator.

In thermal equilibrium, the coherences between the states are all zero, while the populations of the energy levels obey the Boltzmann distribution. The thermal equilibrium density matrix for isolated spins-1/2 is given by

$$\hat{\rho}_{eq} = \frac{\exp(-\hat{H}_0/k_BT)}{\mathrm{Tr}\left\{\exp(-\hat{H}_0/k_BT)\right\}}, \tag{3.13}$$

where $\hat{H}_0$ is the Hamiltonian in the form of Eq. 3.3 and k_B is the Boltzmann constant.

The density matrix can be rewritten in an approximate form of

$$\hat{\rho}_{eq} \approx \begin{pmatrix} \frac{1}{2}+\frac{1}{4}\mathbb{B} & 0 \\ 0 & \frac{1}{2}-\frac{1}{4}\mathbb{B} \end{pmatrix} = \frac{1}{2}\hat{1} + \frac{1}{2}\mathbb{B}\hat{I}_z, \tag{3.14}$$

where $\hat{1}$ is the unity operator and $\mathbb{B}$ is the *Boltzmann factor* defined as

$$\mathbb{B} = \frac{\gamma\hbar B_0}{k_BT}. \tag{3.15}$$

This means that, for positive γ, the low-energy state $|\alpha\rangle$ is populated slightly more than the high-energy state $|\beta\rangle$. Since $\mathbb{B}$ is a very small number, the population difference is exceedingly small at ordinary temperatures and fields.

Therefore, the polarization of the spin angular momentum vectors along the direction of the external field in thermal equilibrium is very slight.

A consequence of this fact is the very low sensitivity of NMR compared to other spectroscopic techniques. Nevertheless, several approaches to deal with this fact were developed, including usage of very high static fields, signal averaging, isotopic enrichment of samples, polarization transfer, etc.

3.1.3 Magnetization vector

Consistent with the population difference between the spin energy levels, one can introduce the ensemble averaged nuclear magnetic moment, or *magnetization vector* $\boldsymbol{M}$, indicating the magnitude and the direction of the net magnetic moment. The three Cartesian components of the vector are

$$M_z = \frac{2}{\mathbb{B}}\left(\rho_{\alpha\alpha} - \rho_{\beta\beta}\right) \tag{3.16}$$

$$M_x = \frac{4}{\mathbb{B}}\mathrm{Re}\left\{\rho_{\beta\alpha}\right\} \tag{3.17}$$

$$M_y = \frac{4}{\mathbb{B}}\mathrm{Im}\left\{\rho_{\beta\alpha}\right\}, \tag{3.18}$$

where "Re" and "Im" denote the real and imaginary part of the density matrix elements, respectively. Clearly, the net magnetization is parallel to the direction of the external magnetic field (z-axis) in thermal equilibrium.

It is possible to investigate the response of the magnetization vector to the r.f. field $\boldsymbol{B}_{RF}$ in analogy to the case of the single spin-1/2, described in Section 3.1.1. It can be shown that, consistently with the single-spin case, the r.f. field causes the rotation of the magnetization vector around the direction of $\boldsymbol{B}_{RF}$ by the angle defined by the strength and length of the pulse.

3.1.4 Bloch equations

It is experimentally observed that, after the perturbation of the spin system, the populations gradually drift towards their thermal equilibrium values and the coherences gradually decay to zero. These observations are due to the *nuclear spin relaxation*. The phenomenological approach to the spin relaxation describes the dynamics of the magnetization in terms of Bloch equations [30]

$$\frac{\mathrm{d}M_z}{\mathrm{d}t} = \gamma(\boldsymbol{M}\times\boldsymbol{B})_z - \frac{M_z - M_0}{T_1} \tag{3.19}$$

$$\frac{\mathrm{d}M_x}{\mathrm{d}t} = \gamma(\boldsymbol{M}\times\boldsymbol{B})_x - \frac{M_x}{T_2} \tag{3.20}$$

$$\frac{\mathrm{d}M_y}{\mathrm{d}t} = \gamma(\boldsymbol{M}\times\boldsymbol{B})_y - \frac{M_y}{T_2}. \tag{3.21}$$

Eq. 3.19 predicts the magnetization component along the $\boldsymbol{B}_0$ to decay to its equilibrium value, M_0. The time constant for this process is called the *longitudinal*, or *spin-lattice*, relaxation time T_1. The solution to Eq. 3.19 after the initial inversion of magnetization by a π-pulse can be written in the form of an exponentially recovering function

$$M_z(t) = M_0\,(1 - 2\exp(-t/T_1))\,. \tag{3.22}$$

Equations 3.20 and 3.21 describe the exponential decay of the transverse components of the magnetization, M_x and M_y, to zero. This process is characterized by the *transverse*, or *spin-spin*, relaxation time constant T_2. The evolution of the transverse components of the magnetization vector after the $\pi/2$-pulse is expressed as

$$M_{x,y}(t) = M_0 \exp(-t/T_2). \tag{3.23}$$

Sometimes, the reciprocal values of T_1 and T_2, denoted *relaxation rates* R_1 and R_2, are used.

The reason for introducing two different time constant is the different physical origin of the transverse and longitudinal relaxation. The longitudinal relaxation involves the energy exchange between the spin system and the surrounding matter ("lattice"), while the transverse relaxation involves the loss of phase coherence in the motion of individual spins. We shall discuss the relaxation phenomenon in detail further in Section 3.5.

3.2 NMR interactions

A real sample contains a large number of electrons as well as nuclei. The nuclear spins not only experience the external magnetic field, but also interact with each other and with the electrons present.

The complete description of the dynamics of nuclei and electrons is nearly impossible and, fortunately, not necessary. In order to describe the dynamics of the spins, one can use the nuclear spin Hamiltonian, which only describes the spin states of the nuclei, and enters the time-dependent Schrödinger equation. Further simplifications are possible, since the internal interactions of the spins are usually much weaker compared to the interactions with the external field. Therefore, in most cases, they can be treated in terms of perturbation theory as a perturbation to the Zeeman Hamiltonian.

The effect of the spin interactions can be observed at two stages. The first one is their effect on NMR spectra, second is their influence on the spin relaxation.

Here we describe the most relevant interactions and their Hamiltonians involved in diamagnetic systems of spins-1/2.

3.2.1 Chemical shift

The electrons surrounding nuclei cause the local magnetic field to vary on a sub-molecular distance scale. The external magnetic field induces electron currents that generate a local magnetic field proportional to the static magnetic field, but not necessarily in the same direction. The magnetic moments of the spins react to the field induced by these electronic currents. The Hamiltonian for the response of a single spin I to the induced magnetic field is

$$\hat{H}_{CS} = \gamma \hat{\boldsymbol{I}} \cdot \boldsymbol{\sigma} \cdot \boldsymbol{B}_0. \tag{3.24}$$

The quantity $\boldsymbol{\sigma}$ is called the *chemical shift tensor*. It is a property of a particular nucleus and it is in general anisotropic.

As any rank-2 Cartesian tensor, the shielding tensor can be decomposed into its symmetric and antisymmetric part. The coordinate system, in which the symmetric part has only diagonal elements σ_{XX}, σ_{YY}, and σ_{ZZ}, is called the *principal axis system*. The isotropic component of the symmetric chemical shift tensor σ_{iso} is called the *isotropic chemical shift* and it is defined as

$$\sigma_{iso} = \frac{1}{3}\left(\sigma_{XX} + \sigma_{YY} + \sigma_{ZZ}\right). \tag{3.25}$$

The choice of the principal axis system follows usually the convention

$$\left|\sigma_{ZZ} - \sigma_{iso}\right| \geq \left|\sigma_{XX} - \sigma_{iso}\right| \geq \left|\sigma_{YY} - \sigma_{iso}\right|. \tag{3.26}$$

We can also define a quantity $\Delta\sigma$ denoted the *chemical shift anisotropy* (CSA) as

$$\Delta\sigma = \sigma_{ZZ} - \frac{1}{2}\left(\sigma_{XX} + \sigma_{YY}\right). \tag{3.27}$$

The case of non-zero CSA reflects the fact that the shielding experienced by a particular nucleus depends on the orientation of the molecule bearing the nucleus with respect to the static magnetic field.

In the case of isotropic liquids, only the isotropic component σ_{iso} is important due to the motional averaging. As a consequence of the chemical shift, the Larmor frequency of the nuclei in the isotropic liquids is shifted to the value

$$\omega_0^{CS} = -\gamma B_0\left(1 + \sigma_{iso}\right), \tag{3.28}$$

causing different positions of the resonances of the nuclei with the different electronic environment in NMR spectra.

The absolute magnitude of the chemical shift is dependent on the magnitude of the external magnetic field B_0, therefore it is convenient to introduce a relative scale independent of the measuring apparatus as

$$\delta_{iso}[\text{ppm}] = \frac{\omega_0 - \omega_{st}}{\omega_{st}} \times 10^6 = \frac{\sigma_{st} - \sigma_{iso}}{1 - \sigma_{st}} \times 10^6 \approx (\sigma_{st} - \sigma_{iso}) \times 10^6, \quad (3.29)$$

where ω_0 is the Larmor frequency of the particular isotope and ω_{st} is the Larmor frequency of a reference compound. For experiments on ^{1}H and ^{13}C nuclei, a common reference compound is the *tetramethylsilane* (TMS), $Si(CH_3)_4$.

The chemical shift range differs for different isotopes in correlation with their number of electrons. For the ^{1}H nuclei, the chemical shift can vary in tens of ppm depending on the electronic environment. For heavier nuclei, like ^{13}C, the chemical shift can range in hundreds of ppm.

3.2.2 Direct dipole-dipole interaction

The strongest interaction for 1/2-spin nuclei is the *direct dipole-dipole (DD) interaction*. This interaction arises between two nuclear magnetic moments close to each other in space. Each of the magnetic moments generates a magnetic field to which the other spin responds. The direct dipole-dipole interaction between spins I and S is represented by the Hamiltonian of the following form

$$\hat{H}_{DD} = b_{IS} \left[3(\hat{\boldsymbol{I}} \cdot \boldsymbol{e})(\hat{\boldsymbol{S}} \cdot \boldsymbol{e}) - \hat{\boldsymbol{I}} \cdot \hat{\boldsymbol{S}} \right], \quad (3.30)$$

where $\boldsymbol{e}$ is the unit vector in the direction of the line connecting the two nuclei. The magnitude of the dipole-dipole coupling is given by the *dipole-dipole coupling constant*, usually denoted b_{IS} and given by:

$$b_{IS} = -\frac{\mu_0 \gamma_I \gamma_S \hbar}{4\pi r_{IS}^3}, \quad (3.31)$$

where the distance between the two spins is r_{IS}, and γ_I and γ_S are their magnetogyric ratios.

In the case of isotropic liquids, the dipole-dipole interaction vanishes due to the molecular tumbling, which changes the orientation of the IS-spin axis on a time scale much faster compared to the dipole-dipole couplings. The dipole-dipole interaction therefore does not influence the appearance of liquid spectra. However, it plays an important role in nuclear spin relaxation.

3.2.3 J-coupling

The indirect dipole-dipole interaction, or *J-coupling*, is an interaction between two nuclear spins mediated by chemical bond electrons. Two spins have a measurable J-coupling if they are connected through a small number of chemical

bonds, including hydrogen bonds. Therefore, the J-coupling provides a direct spectral manifestation of the chemical bond and is an important connection between NMR and chemistry. The full form of the intramolecular J-coupling interaction between the two spins I and S is

$$\hat{H}_J = 2\pi\, \hat{\boldsymbol{I}} \cdot \boldsymbol{J}_{IS} \cdot \hat{\boldsymbol{S}}, \tag{3.32}$$

where $\boldsymbol{J}_{IS}$ is the *J-coupling tensor*, which depends on the molecular orientation. In isotropic liquids, the J-coupling tensor is averaged by the rapid molecular tumbling and attains the isotropic form given as the trace of $\boldsymbol{J}_{IS}$

$$J_{IS} = \frac{1}{3}\left(J_{xx} + J_{yy} + J_{zz}\right). \tag{3.33}$$

The scalar constant J_{IS} is sometimes referred to as the *scalar coupling constant*. Unlike the chemical shift, J-coupling is independent of the external magnetic field.

3.3 Translational diffusion

Molecules, or generally any particles, in solution are randomly changing their positions due to the Brownian motion. This phenomenon is known as the *translational diffusion*. It is characterized by the *translational diffusion coefficient* D, defined according to the Stokes-Einstein theory [31] as

$$D = \frac{k_B T}{f_T}, \tag{3.34}$$

where f_T is the *friction factor*, given by

$$f_T = 6\pi\eta r_H \tag{3.35}$$

for the special case of a spherical particle of hydrodynamic radius r_H in a solvent of viscosity η. Combining Equations 3.34 and 3.35, it is possible to express the hydrodynamic radius as

$$r_H = \frac{k_B T}{6\pi\eta D}. \tag{3.36}$$

Pulse-field gradient (PFG) NMR spectroscopy can be used to measure the translational diffusion of molecules. By the use of a magnetic field gradient, molecules can be spatially labeled, i.e. marked depending on their position in the sample tube. One of the simplest pulse sequences for measuring the translational diffusion is the *stimulated spin echo* sequence, proposed by Stejskal and Tanner [32].

The principle of the stimulated echo sequence lies in the application of the gradient of the external magnetic field of magnitude G in the direction of the static magnetic field $\boldsymbol{B}_0$. Owing to this gradient, the magnetic field varies along the z-axis according to

$$B(z) = B_0 + G(z), \tag{3.37}$$

and so does the Larmor frequency ω_0 of the nuclei

$$\omega_0(z) = -\gamma(B_0 + G(z)). \tag{3.38}$$

The position of the nuclei along the z-axis is encoded according to their phase angle

$$\phi(z) = -\omega_0(z)\delta = -\gamma B(z)\delta, \tag{3.39}$$

where δ is the duration of the gradient pulse.

The application of the second gradient causes that only spins which did not change their position during the delay Δ between the gradient pulses are refocused and contribute to the signal. The detected signal intensity is attenuated depending on the diffusion coefficient of the species in the sample

$$I_{(2\tau,G)} = I_{(2\tau,0)} e^{-D\gamma^2 G^2 \delta^2 (\Delta - \delta/3)}, \tag{3.40}$$

where $I_{2\tau,G}$ is the intensity of the signal at the time 2τ with the gradient applied, $I_{2\tau,0}$ is the signal intensity at 2τ without applied gradient, and $\Delta - \delta/3$ is the diffusion time. The translational diffusion coefficient D can be obtained by fitting the Gaussian decaying function of Eq. 3.40 to the experimental intensities vs. the gradient strength.

Recently, more elaborate experimental protocols have been developed in order to deal with the drawbacks of the simple stimulated echo. In order to compensate the eddy-current effects, bipolar gradients [33] or the longitudinal eddy-current delay (LED) [34] are used. Convection within the sample is suppressed by the use of the double-stimulated echo [35]. The pulse sequence depicted in Figure 3.1, with the spin-lock before the acquisition to remove minor phase distortions in the spectra [36], was used in this work.

3.4 Two-site chemical exchange

Chemical exchange is in general any process at which the spins in the molecule change their magnetic environment. This may be due to chemical reaction, isomerization, conformational changes, complexation of molecules, etc. These phenomena reflect in NMR spectra and can affect the spin relaxation.

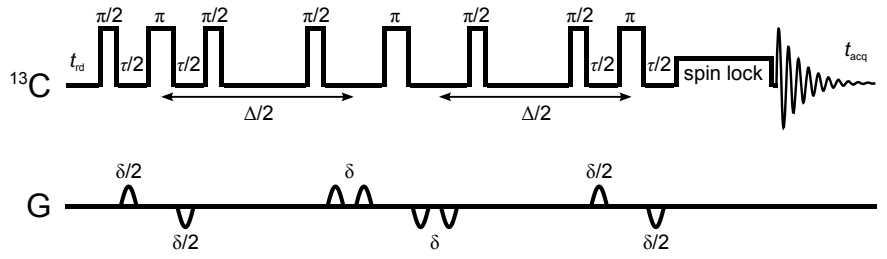

Figure 3.1: A double stimulated spin-echo pulse sequence for measuring the translational diffusion with the bipolar gradient pulses and the spin-lock before the acquisition. Appropriate phase cycling and cleaning gradients have to be used (not shown).

The two-site chemical exchange process, at which the nuclear spin is transported between two sites A and B with unequal chemical shifts ω_A and ω_B, can be characterized by equation

$$A \underset{k_{-1}}{\overset{k_1}{\rightleftharpoons}} B, \tag{3.41}$$

where k_1 and k_{-1} are the first-order *exchange rate constants*. The exchange rates k_1 and k_{-1} may in general differ if the energy barriers for forward and backward reactions are not equal. The ratio of the rate constants is called the *equilibrium constant* and it is equal to the ratio of the equilibrium concentrations of the two species

$$K = \frac{k_1}{k_{-1}} = \frac{[B]_{eq}}{[A]_{eq}}. \tag{3.42}$$

In the case when $k_1 = k_{-1}$, we speak of a symmetrical two-site exchange.

The effect of the chemical exchange depends on the difference in the chemical shifts frequency of the two sites $\Delta\omega = \omega_A - \omega_B$ compared to the exchange rate $k_{ex} = k_1 + k_{-1}$. The spectral lineshapes are most profoundly affected by the exchange process if the system is in the *intermediate exchange* regime where $\Delta\omega$ is similar to k_{ex}.

In the case when

$$k_{ex} < |\Delta\omega/2| \tag{3.43}$$

we speak of the *slow intermediate exchange* regime, in which we observe separate lines for A and B sites at their frequencies ω_A and ω_B. The exchange rates in this regime can be obtained by the 1D NOESY experiment (see Section 3.4.2).

Broadening of the lines occurs with the increase of the exchange rate k_{ex}. The point at which

$$k_{ex} = |\Delta\omega/2| \tag{3.44}$$

is called the cross-over point and approximately corresponds to the point where the spectral lines for the two sites merge to one line, called the *coalescence*. The single peak appears at a position given by the average of the two chemical shifts ω_A and ω_B, weighted by the equilibrium concentrations of the two species.

The *fast intermediate exchange* is characterized by

$$k_{ex} > |\Delta\omega/2| \tag{3.45}$$

and in this regime the further increase of the exchange rate causes narrowing of the single line. The exchange rates in the fast intermediate exchange can be evaluated for example by lineshape analysis [37; 38].

3.4.1 Host-guest complex formation

In this work, the chemical exchange considered is the encapsulation of the molecular guest (G) by the molecular host (H) leading to the *host-guest* (HG) *complex* formation. Thus, the guest is in exchange between the bulk solvent (free state) and the cavity of the host (bound state). The process can be expressed by a chemical reaction

$$H + G \underset{k_{-1}}{\overset{k_1}{\rightleftharpoons}} HG \tag{3.46}$$

with the rate constants k_1 and k_{-1}. For the interpretation of NMR experiments, the effective pseudo-first-order exchange rates for free-to-bound (k_{FB}) and bound-to-free (k_{BF}) reaction are introduced

$$k_{FB} = k_1[H] \tag{3.47}$$
$$k_{BF} = k_{-1} \tag{3.48}$$
$$k_{ex} = k_{FB} + k_{BF}. \tag{3.49}$$

The association equilibrium constant is given according to

$$K = \frac{k_{FB}}{k_{BF}[H]} = \frac{[\mathrm{HG}]}{[\mathrm{H}][\mathrm{G}]}. \tag{3.50}$$

The activation energies of the exchange process E_a can be determined by fitting the Arrhenius equation

$$k(T) = A \exp\left(-\frac{E_a}{\mathbb{N}_A k_B T}\right) \tag{3.51}$$

to the temperature-dependent exchange rate constants, where k stands either for k_1 or k_{-1} and $\mathbb{N}_A$ is the Avogadro constant.

3.4.2 1D NOESY experiment

One of the most powerful aspects of NMR is the ability to detect the chemical exchange phenomena, even when the system is in equilibrium, over a wide range of rates. The exchange rates in the slow intermediate exchange regime can be determined for instance by the one-dimensional NOESY experiment, using the fact that chemical exchange can lead to a magnetization transfer between the two sites in exchange.

The selective 1D NOESY pulse sequence with the pulsed-field gradients [39] is depicted in Figure 3.2. The sequence starts with a selective excitation of one of the sites by a technique termed *excitation sculpting*. This consists of the double pulsed-field gradient spin-echo (DPFGSE), which combines the selective shaped π-pulses with the pulsed-field gradients (g_1–g_3) to dephase the non-desired magnetization. Second part of the sequence contains a variable mixing time delay τ_m, during which the magnetization transfer, caused by the exchange, occurs. The signal is then detected at the second site by the last $\pi/2$-pulse.

The experiment is usually repeated for several suitably chosen values of the mixing time τ_m. As a result, the exchange-mediated intensity buildup as a function of τ_m is obtained. Assuming that the chosen τ_m values are sufficiently short for observing the process in the *initial rate* regime, the reaction rates are given by the slope of the buildup curve [40; 41].

3.5 NMR relaxation

Relaxation is a process of returning of the spin system to the equilibrium after a perturbation. As described in Section 3.1.4, the populations obey the Boltzmann distribution and the coherences are zero in thermal equilibrium.

For spins-1/2, nuclear spin relaxation is caused by a fluctuating magnetic field at the sites of the nuclear spins. The fluctuating field originates from the weak magnetic interactions in combination with the random thermal motion of the molecules. For diamagnetic systems, the most important sources of the

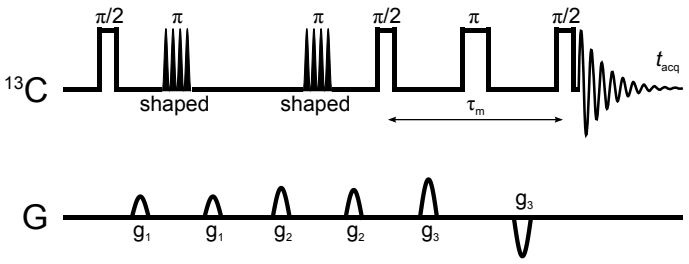

Figure 3.2: The 1D NOESY sequence with double pulsed-field gradient spin-echo (DPFGSE) for determining the chemical exchange rates. Appropriate phase cycling has to be used (not shown).

fluctuating field are the direct dipole-dipole interaction and the chemical shift anisotropy.

A useful way to describe the relaxation is therefore in terms of random processes. Consider a stochastic function of time $Y(t)$. The properties of $Y(t)$ at the different times t are in general not independent. A *time-correlation function* can be constructed to investigate the correlation of the stochastic process at two distinct time points separated by delay τ

$$C(\tau) = \langle Y(t)Y^*(t+\tau)\rangle\,, \tag{3.52}$$

where asterisk denotes the complex conjugate. $C(\tau)$ is sometimes also called the *auto-correlation function* to stress the correlation of a stochastic process with itself. For $\tau = 0$, the auto-correlation function is equal to the variance of $Y(t)$

$$C(0) = \langle Y(t)Y^*(t)\rangle = \sigma^2. \tag{3.53}$$

For very long τ, it is reasonable to assume that $Y(t)$ and $Y(t+\tau)$ are uncorrelated and $C(\tau)$ decays to zero

$$\lim_{\tau\to\infty} C(\tau) = 0. \tag{3.54}$$

The simplest choice is to assume that $C(\tau)$ is an exponentially decaying function

$$C(\tau) = C(0)e^{-|\tau|/\tau_c}, \tag{3.55}$$

where τ_c is called the *correlation time*, which reflects the time scale of the random field fluctuations.

An important role in relaxation theory is played by the *spectral density function* $J(\omega)$, given by the Fourier transform of the correlation function $C(\tau)$

$$J(\omega) = \int_{-\infty}^{\infty} C(\tau)e^{-i\omega\tau}\mathrm{d}\tau. \tag{3.56}$$

The spectral density function represents the amount of the radio-frequency power generated by the stochastic process $Y(t)$ at a particular frequency ω. For the time-correlation function in the form of 3.55, the spectral density is a Lorentzian function:

$$J(\omega) = C(0)\frac{2\tau_c}{1+\omega^2{\tau_c}^2}. \tag{3.57}$$

For the relaxation through rank-2 interactions (such as dipole-dipole interaction or chemical shift anisotropy), a time correlation function for the normalized rank-2 spherical harmonics ($Y_{l,m}$ with $l = 2$) is required. For $Y(t)$ in the form of

$$Y_{2,0}(t) = \frac{1}{4}\sqrt{\frac{5}{\pi}}\left[3\cos^2\theta(t) - 1\right] \tag{3.58}$$

it can be shown that the relevant time correlation function for the small-step rotational diffusion of isotropically reorienting rigid body is indeed in the form of a simple exponential

$$C_2(\tau) = \frac{1}{4\pi}e^{-\tau/\tau_c} \tag{3.59}$$

with $\tau_c = \frac{1}{6D_R}$, where D_R is the rotational diffusion coefficient.

In most of other cases dealing with more complex dynamics, including flexible molecules, more complicated expressions for $J(\omega)$ have to be employed (see Section 3.8).

3.5.1 Relaxation through dipole-dipole interactions

For spins-1/2, the most important relaxation mechanism is the dipole-dipole interaction between the nuclear magnetic moments of the spins in the spatial vicinity of each other. The dipolar relaxation parameters are also an important source of information about molecular dynamics.

Consider a situation with a solution containing molecules with two types of nuclear spins-1/2, denoted I and S. We assume that no J-couplings are present, only the dipole-dipole interaction between the spins. The system is described by four Zeeman energy levels and a set of transition probabilities between the levels (see Figure 3.3). One can set up a set of equations describing the kinetics of the populations in the four-level system. It was shown by Solomon [42] that the relaxation of the longitudinal magnetization components, proportional to the expectation values of the $\hat{I}_z$ and $\hat{S}_z$ operators, is related to the populations of the four-level system and can be described by a set of following equations, denoted *Solomon equations*

$$\frac{\mathrm{d}}{\mathrm{d}t}\begin{bmatrix}\langle\hat{I}_z\rangle\\ \langle\hat{S}_z\rangle\end{bmatrix} = -\begin{bmatrix}\rho_I & \sigma_{IS}\\ \sigma_{IS} & \rho_S\end{bmatrix}\begin{bmatrix}\langle\hat{I}_z\rangle - I_z^{eq}\\ \langle\hat{S}_z\rangle - S_z^{eq}\end{bmatrix}, \tag{3.60}$$

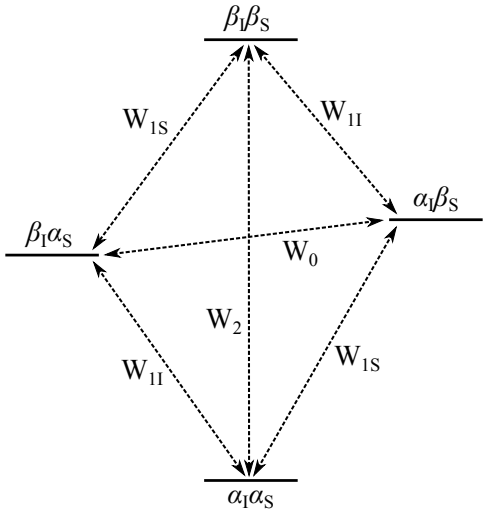

Figure 3.3: The energy-level diagram associated with a two-spin system

where I_z^{eq} and S_z^{eq} are the equilibrium longitudinal magnetizations of the two spins, and ρ_I and ρ_S are corresponding longitudinal relaxation rates. The symbol σ_{IS} denotes the *cross-relaxation rate*. The matrix at the right-hand side of Eq. 3.60 is called the *relaxation matrix*. The relaxation rates are associated with the transition probabilities in the following way

$$\rho_I = W_0 + 2W_{1I} + W_2 \tag{3.61}$$

$$\rho_S = W_0 + 2W_{1S} + W_2 \tag{3.62}$$

$$\sigma_{IS} = W_2 - W_0 \tag{3.63}$$

The Solomon approach uses the time-dependent perturbation theory to derive the transition probabilities between the pairs of energy levels in Figure 3.3. The transition probabilities, induced by a random process, are proportional to spectral densities of the random perturbation evaluated at the relevant frequencies:

$$W_{1I} = \frac{3\pi}{10} b_{IS}^2 J(\omega_I) \tag{3.64}$$

$$W_{1S} = \frac{3\pi}{10} b_{IS}^2 J(\omega_S) \tag{3.65}$$

$$W_0 = \frac{\pi}{5} b_{IS}^2 J(\omega_I - \omega_S) \tag{3.66}$$

$$W_2 = \frac{\pi}{5} b_{IS}^2 J(\omega_I + \omega_S). \tag{3.67}$$

The relaxation equations for the spins I and S are coupled by the cross-relaxation term σ_{IS} and thus the general solution to the Eq. 3.60 for $\langle \hat{I}_z \rangle$ and $\langle \hat{S}_z \rangle$ is a sum of two exponentials. Although the cross-relaxation is in principle always present in dipolar-relaxed systems, the single exponential behavior, postulated by Bloch (Eq. 3.22), can be obtained under certain conditions. Such conditions can be achieved, for instance, by irradiation of the I-spin with a radio-frequency field at its resonant frequency. The relaxation rate of the S-spin in such case is given by

$$T_{1S}^{-1} \equiv \rho_S = W_0 + 2W_{1S} + W_2. \tag{3.68}$$

This situation applies, for example, for carbon-13 (S-spin) relaxation under the broad-band decoupling of protons (I-spins).

The irradiation of the spin I, leading to its saturation ($\langle \hat{I}_z \rangle = 0$), results also in the modification of the steady-state ($\mathrm{d}\langle \hat{S}_z \rangle / \mathrm{d}t = 0$) solution to the Solomon equations for the spin S

$$\langle \hat{S}_z \rangle_{steady-state} = S_z^{eq}(1+\eta). \tag{3.69}$$

The steady-state intensity of the S-spin signal is enhanced by a factor of $(1+\eta)$, where

$$\eta = \frac{\gamma_I}{\gamma_S}\frac{\sigma_{IS}}{\rho_S}. \tag{3.70}$$

This phenomenon is referred to as the *Nuclear Overhauser Effect* (NOE) and the quantity $(1+\eta)$ is called the *NOE enhancement factor*. If the spins I and S are of different isotopic species (as for example ^{13}C and ^{1}H), we talk about the *heteronuclear* NOE. Measurement of the enhancement factor allows for determination of the cross-relaxation rate σ_{IS}. This relaxation parameter carries information on the relaxation mechanisms and on the molecular dynamics.

3.5.2 Carbon-13 relaxation

The main focus in this work has been put on carbon-13 NMR relaxation parameters, since they contain valuable information about the dynamics or structure of the molecules.

For ^{13}C nuclei directly bonded to one or more hydrogens, the dipole-dipole interaction with these hydrogens is normally the dominant relaxation mechanism. Application of a proton broadband decoupling removes not only the J-coupling with the attached protons, but also the coupling between the two relaxation equations in Eq. 3.60. Thus, the longitudinal carbon-13 relaxation is mono-exponential (well-defined T_1) and the NOE factor is always positive.

Under the assumptions of the Solomon approach, i.e. only dipole-dipole interaction between ^{1}H and ^{13}C present, one can obtain expression for T_1 and NOE from Eqs. 3.68 and 3.70 combined with Eqs. 3.64–3.67.

Under certain conditions, the transverse relaxation is also mono-exponential and similar expression can be derived for the relaxation time T_2

$$T_{1,\mathrm{DD}}^{-1} = \frac{\pi}{5} b_{CH}^2 \left[J(\omega_H - \omega_C) + 3J(\omega_C) + 6J(\omega_H + \omega_C) \right] \tag{3.71}$$

$$\eta = \frac{\gamma_H}{\gamma_C} \frac{6J(\omega_H + \omega_C) - J(\omega_H - \omega_C)}{J(\omega_H - \omega_C) + 3J(\omega_C) + 6J(\omega_H + \omega_C)} \tag{3.72}$$

$$\begin{aligned} T_{2,\mathrm{DD}}^{-1} = {} & \frac{\pi}{10} b_{CH}^2 \left[4J(0) + J(\omega_H - \omega_C) + \right. \\ & \left. + \; 3J(\omega_C) + 6J(\omega_H) + 6J(\omega_H + \omega_C) \right]. \end{aligned} \tag{3.73}$$

The dipole-dipole coupling constant b_{CH} for $I =^1$H and $S =^{13}$C is defined in Eq. 3.31. For a rigid molecule, b_{CH} is proportional to the inverse cube of the C-H distance r_{CH}. Sometimes, the vibrationally averaged r_{CH} distance has to be used to account for the effect of molecular vibrations [43].

The simple form of the relaxation parameters in Eqs. 3.71–3.73 in the presence of the proton decoupling may be retained also for more complicated spin systems. For a carbon-13 interacting with two non-equivalent protons, it is sufficient to multiply the Eqs. 3.71 and 3.73 by a factor of two.

The relaxation parameters T_1, T_2 and NOE are commonly referred to as the "conventional" relaxation parameters, in contrast with the cross-correlated relaxation parameters that will be discussed in Section 3.7.

From the experimental point of view, it is important to notice the dependence of the relaxation parameters in Eqs. 3.71–3.73 on the magnetic field strength (through ω_H and ω_C). For a given correlation time τ_c, in a region where $\omega^2\tau_c^2 \ll 1$, the relaxation parameters are practically independent of the external field. This region is called the *extreme narrowing* regime. On the other hand, a field-dependence of relaxation parameters for $\omega^2\tau_c^2 \geq 1$ is observed. Note that ω represents here all the relevant frequencies that enter the spectral densities $J(\omega)$ in Eqs. 3.71–3.73, the largest being $\omega_H + \omega_C$.

Carbon-13 relaxation parameters outside of the extreme narrowing regime can provide an excellent source of information on molecular dynamics in solution.

We can also investigate the dependence of $1/T_1$ and $1/T_2$ on the correlation time τ_c and through this also on molecular size, solvent viscosity and temperature. Under the extreme narrowing conditions, T_1 and T_2 are equal. Outside of the extreme narrowing regime, $1/T_1$ reaches its maximum and further decreases with rising τ_c, while $1/T_2$ is rising instead.

3.6 Measuring relaxation parameters

3.6.1 Inversion – recovery: T_1 measurement

The spin-lattice relaxation time T_1 can be determined by using the *inversion – recovery* pulse sequence (see, for example, [27]), which is depicted in Figure 3.4. The pulse sequence begins with a π_x-pulse which generates an inverted population distribution, i.e. inverts the magnetization. The populations relax back to the thermal equilibrium during the recovery delay τ. The final $(\pi/2)_x$-pulse converts the population differences into observable coherences (transverse magnetization). A recycle delay t_{rd} should be long enough (approximately 5-times T_1) to ensure the equilibrium conditions between the repetitions of the experiment.

T_1 can be determined by repeating the experiment for different recovery delays τ and fitting the exponentially recovering function of type as in Eq. 3.22 to the experimental peak intensities vs. relaxation delays.

For carbon-13 T_1 experiments, decoupling of protons throughout the measurement is usually applied to ensure that the relaxation is mono-exponential.

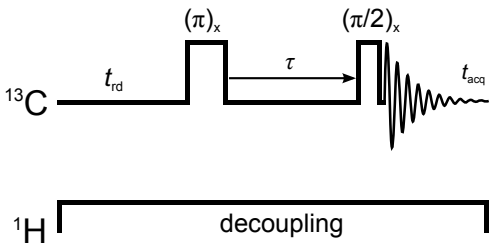

Figure 3.4: The inversion – recovery pulse sequence for measuring the relaxation time T_1.

3.6.2 Spin-echo: T_2 measurement

The basic spin-echo sequence, proposed by Hahn [44], consists of a $(\pi/2)_x$-pulse followed by a π_x-pulse, separated by a delay $\tau/2$, where τ is the echo time. The first pulse creates the transverse magnetization, which is let to evolve for a period of $\tau/2$. The contribution of different spins evolve with different rates due to the chemical shift differences, or possible inhomogeneities of the magnetic field. After this period, the magnetization in the *xy*-plane is inverted by the π-pulse. Another $\tau/2$ after the second pulse, transverse magnetization is refocused and a spin-echo is observed.

A modification of the simple spin-echo sequence was proposed by authors Carr and Purcell [45], and Meiboom and Gill [46], also referred to as the *CPMG sequence*, depicted in Figure 3.5. The modified sequence uses *y*-phase π-pulses and the variation of the relaxation delay is ensured by repeating the ($\tau/2$ – π-pulse – $\tau/2$) *n*-times with a short constant delay τ. The experiment is repeated for variable *n* and spectra are analyzed by fitting the exponentially decaying function of type as in Eq. 3.23 to the signal intensity dependence on the number of cycles to obtain the T_2 relaxation time. On the proton channel, a suitably placed π-pulse is used to suppress the cross-correlation effects (discussed in Section 3.7) between the carbon-13 CSA and proton – carbon-13 dipole-dipole interaction [47; 48].

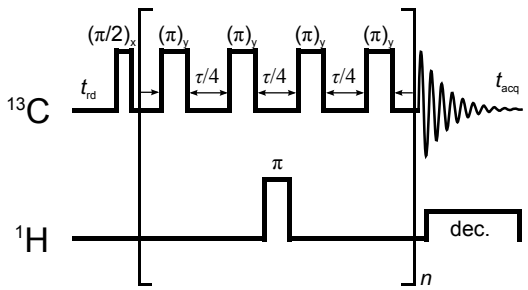

Figure 3.5: The CPMG spin-echo pulse sequence for measuring the relaxation time T_2.

3.6.3 Steady-State NOE

Heteronuclear steady-state NOE enhancement factor can be obtain through two separate experiments (Figure 3.6) [27]. In the first experiment, protons are continuously irradiated during a delay τ, which must be sufficiently long to ensure that the NOE is built up to the maximum value. Then a $\pi/2$-pulse is applied and the signal acquisition follows. The second experiment is performed without the irradiation. Broadband decoupling of protons is used during the acquisition. It is important to attain a complete relaxation of the magnetization between the scans in order to obtain the correct intensities. Typically, a delay of approximately 10-times T_1 is used. The steady-state NOE factor is obtained as the ratio of the signal intensities obtained by these two experiments.

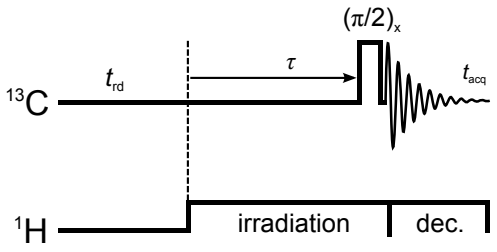

Figure 3.6: Steady-state NOE pulse sequence.

3.7 Cross-correlated relaxation

3.7.1 Redfield relaxation theory

The Solomon approach to the relaxation is limited to a two-spin system coupled through the dipole-dipole interaction. This can be a limitation if one needs to deal with multi-spin systems or other sources of relaxation than the dipole-dipole interaction. A more general formulation of the relaxation theory, suitable also for systems with J-couplings, was proposed by Wangsness, Bloch and Redfield, also known as the *Redfield theory* [49; 50].

The Redfield formulation is in principle applicable to any kind of non-equilibrium system with any relaxation mechanism. It is based on the second-order time-dependent perturbation theory and it is given in terms of density matrix evolution, described by the Liouville – von Neumann equation.

The relaxation Hamiltonian considered in the Redfield theory is a sum of the time-independent part $\hat{H}_0$ (the main Hamiltonian) and the stochastic time-dependent part $\hat{H}_1(t)$ (the perturbation Hamiltonian). A comprehensive derivation of the Redfield theory can be found in the book of Abragam [28] in terms of the operator formalism and in the book of Slichter [29] in terms of the eigenstate formulation. Here we limit ourselves to present the main results.

The equation for the time evolution of density matrix elements in Redfield theory is based on the Liouville – von Neumann equation and takes the form of

$$\frac{\mathrm{d}\rho_{\alpha\alpha'}}{\mathrm{d}t} = -i\omega_{\alpha\alpha'}\rho_{\alpha\alpha'} + \sum_{\beta,\beta'} R_{\alpha\alpha'\beta\beta'}\,\rho_{\beta\beta'}, \tag{3.74}$$

where $R_{\alpha\alpha'\beta\beta'}$ are the *relaxation supermatrix elements* expressed in the basis of the eigenstates of the unperturbed Hamiltonian $\hat{H}_0$ (α, α', β, β', ...), and $\omega_{\alpha\alpha'}$ represents the energy level separation between the corresponding eigenstates. The $R_{\alpha\alpha'\beta\beta'}$ terms are composed as a linear combination of the spectral

densities at different transition frequencies

$$R_{\alpha\alpha'\beta\beta'} = \frac{1}{2}[\mathtt{J}_{\alpha\beta\alpha'\beta'}(\omega_{\alpha'\beta'}) + \mathtt{J}_{\alpha\beta\alpha'\beta'}(\omega_{\alpha\beta}) - \\ - \delta_{\alpha'\beta'}\sum_{\gamma}\mathtt{J}_{\gamma\beta\gamma\alpha}(\omega_{\gamma\beta}) - \delta_{\alpha\beta}\sum_{\gamma}\mathtt{J}_{\gamma\alpha'\gamma\beta'}(\omega_{\gamma\beta'})], \tag{3.75}$$

where the spectral densities are in the form of

$$\mathtt{J}_{\alpha\alpha'\beta\beta'}(\omega) = 2\int_0^{\infty}\mathtt{G}_{\alpha\alpha'\beta\beta'}(\tau)\exp(-i\omega\tau)\mathrm{d}\tau \tag{3.76}$$

with the time-correlation function $\mathtt{G}_{\alpha\alpha'\beta\beta'}(\tau)$ defined as

$$\mathtt{G}_{\alpha\alpha'\beta\beta'}(\tau) = \overline{\langle\alpha\left|\hat{H}_1(t)\right|\alpha'\rangle\langle\beta\left|\hat{H}_1(t+\tau)\right|\beta'\rangle}, \tag{3.77}$$

where the horizontal bar denotes the ensemble average.

3.7.2 Relaxation interference

When dealing with multi-spin systems, a situation, in which the relaxation of one spin is caused by more than a single relaxation mechanism, can arise. If the stochastic processes causing the relaxation are modulated by the same dynamic process, the interference between the interactions needs to be considered. This effect is also called the *cross-correlation* and was subject of several studies, one of the more recent is the review of Kumar [51].

In this section we demonstrate the application of the Redfield theory to systems consisting of more than two spins with mutual dipole-dipole and scalar interactions. The unperturbed Hamiltonian $\hat{H}_0$ consists of the Zeeman interactions between all the spins and the magnetic field, and also the J-couplings within the spin pairs. The perturbation Hamiltonian $\hat{H}_1(t)$ is a sum of the dipole-dipole interactions over all the η pairs of the nuclei

$$\hat{H}_1(t) = \sum_{\eta}\hat{H}_{\eta}. \tag{3.78}$$

The time-correlation function in Eq. 3.77 thus has to be extended to contain terms correlating different components of the Hamiltonian 3.78

$$\mathtt{G}_{\alpha\alpha'\beta\beta'}(\tau) = \sum_{\eta}\overline{\langle\alpha\left|\hat{H}_{\eta}(t)\right|\alpha'\rangle\langle\beta\left|\hat{H}_{\eta}(t+\tau)\right|\beta'\rangle} + \tag{3.79}$$

$$+ \sum_{\eta\neq\eta'}\overline{\langle\alpha\left|\hat{H}_{\eta}(t)\right|\alpha'\rangle\langle\beta\left|\hat{H}_{\eta'}(t+\tau)\right|\beta'\rangle}, \tag{3.80}$$

where the first term is the auto-correlation function and the second term, where the summation runs over $\eta \neq \eta'$, is called the *cross-correlation function*. The Fourier transform of the cross-correlation function gives the *cross-correlated spectral density*. The cross-correlated spectral densities affect the relaxation properties of the multi-spin systems.

3.7.3 Cross-correlated relaxation in AMX systems

An interesting example to study is the relaxation of the system consisting of three different spins-1/2, denoted the *AMX system*. The three spins are assumed to be coupled to each other by scalar couplings J_{AM}, J_{AX}, and J_{MX}. The unperturbed Hamiltonian H_0 of such a system contains Zeeman interaction for all three spins and their mutual J-couplings and has eight non-degenerate eigenstates.

The NMR spectrum of the AMX system, under the weak-coupling limit assumption, consists of three groups of signals, each group is a symmetric doublet of doublets.

It is convenient to investigate the relaxation matrix of AMX system in the basis of so-called *magnetization modes* υ_i, created as a symmetric (${}^s\upsilon_i$) and antisymmetric (${}^a\upsilon_i$) linear combination of the ket-bra products of the H_0 eigenstates [52]. The advantage of the magnetization mode formulation is that all the elements υ_i are related to observable quantities, for example

$$ {}^a\upsilon_1 = \left\langle \hat{I}_z^A \right\rangle \tag{3.81} $$

$$ {}^a\upsilon_2 = \left\langle \hat{I}_z^M \right\rangle \tag{3.82} $$

$$ {}^a\upsilon_3 = \left\langle \hat{I}_z^X \right\rangle \tag{3.83} $$

$$ {}^a\upsilon_4 = \left\langle 4\hat{I}_z^A \hat{I}_z^M \hat{I}_z^X \right\rangle. \tag{3.84} $$

The first three antisymmetric modes correspond to the expectation values of the $\hat{I}_z$ operators of the three spins. The fourth mode corresponds to the so-called multiplet asymmetry defined as the difference between the summed intensities of the inner lines and outer lines of the multiplet.

The relaxation matrix for the magnetization modes can be formulated in terms of the Redfield theory. Under the assumption of the dipole-dipole interactions between the spins as the only relaxation mechanism, the antisymmetric and the symmetric magnetization modes are not connected by the relaxation matrix and the relaxation matrix is symmetric. We can write

$$ \frac{\mathrm{d}}{\mathrm{d}t} \begin{bmatrix} {}^a\upsilon(t) \\ {}^s\upsilon(t) \end{bmatrix} = - \begin{bmatrix} {}^a\Gamma & 0 \\ 0 & {}^s\Gamma \end{bmatrix} \begin{bmatrix} {}^a\upsilon(t) - {}^a\upsilon^{eq} \\ {}^s\upsilon(t) - {}^s\upsilon^{eq} \end{bmatrix}. \tag{3.85} $$

The first three antisymmetric magnetization modes, the diagonal elements ${}^a\Gamma_{ii}$, correspond to the sum of the two longitudinal relaxation rates of the pairs of the spins

$$ {}^a\Gamma_{11} = \rho_{AM} + \rho_{AX}, \quad {}^a\Gamma_{22} = \rho_{AM} + \rho_{MX}, \quad {}^a\Gamma_{33} = \rho_{MX} + \rho_{AX}. \tag{3.86} $$

Likewise, the off-diagonal elements are identified with the cross-relaxation rates

$$ {}^a\Gamma_{12} = \sigma_{AM}, \quad {}^a\Gamma_{13} = \sigma_{AX}, \quad {}^a\Gamma_{23} = \sigma_{MX}. \tag{3.87} $$

The terms ρ and σ are expressed as linear combinations of the auto-correlated spectral densities $J_{AM,AM}$, $J_{AX,AX}$, and $J_{MX,MX}$, in analogy with Eq. 3.71 and 3.72.

The nature of the elements ${}^a\Gamma_{14}$, ${}^a\Gamma_{24}$, and ${}^a\Gamma_{34}$ is different. They are coupling together the $\hat{I}_z$ terms with the three-spin order term $\langle 4\hat{I}_z^A\hat{I}_z^M\hat{I}_z^X\rangle$ and they depend only on the cross-correlated spectral densities $J_{AM,AX}$, $J_{AM,MX}$, and $J_{MX,AX}$ as

$$ {}^a\Gamma_{14} = \delta_{A,AMX} = \frac{6\pi}{5} b_{AM} b_{AX} J_{AM,AX}(\omega_A) \tag{3.88} $$

$$ {}^a\Gamma_{24} = \delta_{M,AMX} = \frac{6\pi}{5} b_{AM} b_{MX} J_{AM,MX}(\omega_M) \tag{3.89} $$

$$ {}^a\Gamma_{34} = \delta_{X,AMX} = \frac{6\pi}{5} b_{MX} b_{AX} J_{MX,AX}(\omega_X). \tag{3.90} $$

These relaxation rates are thus denoted the longitudinal dipolar *cross-correlated relaxation rates* (CCRRs).

Similarly, we can investigate the cross-correlation between the dipole-dipole interaction and the chemical shift anisotropy and expressions for DD–CSA cross-correlated relaxation rates can be derived. The relaxation interference effects also influence the transverse relaxation. Detailed description of these aspects can be found for example in [27].

An important example of AMX system is a methylene group with carbon-13 (A) and two magnetically non-equivalent protons (M, X). In such a system, the carbon-proton J-couplings are usually of similar magnitude and the carbon-13 spectrum takes a form of a triplet. The dipole-dipole longitudinal CCRRs can be obtained using the experimental protocol described by Ghalebani [53] from a simple ^{13}C inversion – recovery experiment (as described in Section 3.6.1) performed without the decoupling. The relaxation rates in the initial approach (i.e. only for short inversion – recovery delays) are obtained separately for each line of the triplet, denoted W_0^+ and W_0^- for the outer lines, and W_i for the inner line. The longitudinal dipolar CCRRs are then obtained as

$$ \delta_{A,AMX} = \frac{1}{2}\left(\frac{1}{2}(W_0^+ + W_0^-) - W_i\right). \tag{3.91} $$

Cross-correlated relaxation parameters can provide information about molecular geometry through the angular relation between the principal axes of the two interactions involved in the interference.

3.8 Motional models

Until now, we have introduced the spectral density function in the form of Eq. 3.59 for the simple model describing motion of a randomly reorienting

rigid spherical object. In order to describe the dynamics of more complex objects, one has to employ more complicated spectral density functions of various motional models. An overview of motional models that can be used to interpret the relaxation data can be found for example in papers of Daragan and Mayo [54] or more recent of Jarymowycz and Stone [55].

3.8.1 Lipari-Szabo model

Lipari and Szabo [56; 57] proposed a spectral density function to account for objects with an internal degree of freedom besides the global reorientation. The global motion is assumed to be isotropic, described by the *global correlation time* τ_M. The rate of the local motion is evaluated by an *effective correlation time* τ_e and the spatial restriction is measured by a squared *generalized order parameter* S^2. Lipari-Szabo approach assumes the global motion and the local motion to be independent, or decoupled, by virtue of the former being much slower than the latter ($\tau_M \gg \tau_e$). The Lipari-Szabo spectral density is in the form of a sum of two Lorentzian functions

$$J_{LS}(\omega) = \frac{2}{5}\left[\frac{S^2\tau_m}{1+\omega^2\tau_m^2} + \frac{(1-S^2)\tau}{1+\omega^2\tau^2}\right] \tag{3.92}$$

$$\tau^{-1} = \tau_m^{-1} + \tau_e^{-1}. \tag{3.93}$$

The Lipari-Szabo approach is sometimes referred to as "model-free", because it does not provide any detailed physical picture of the internal motion. Nevertheless, the generalized order parameter S^2 can be in certain cases related to parameters defining a specific motional model. One of such models can be the two-site jump model, which is of a particular interest for instance when studying the dynamics of hydroxymethyl groups in carbohydrates [58]. The two-site jump model describes a situation in which the studied bond vector is assumed to alternate between two fixed orientations characterized by angles γ and $-\gamma$, with populations P and $1-P$. For the two-site jump in hydroxymethyl groups, the generalized order parameter is given as [59]

$$S_j^2 = \frac{1}{9} + \frac{8}{27}\left(1 - 4P(1-P)\sin^2\gamma\right) + \frac{16}{27}\left(1 - 4P(1-P)\sin^2\gamma\right). \tag{3.94}$$

The coefficients of the expression assume tetrahedral symmetry of the H-C-H bond angle. A more general expression can be found in the work of Daragan and Mayo [54]. For an ideal two-site jump ($P = 0.5$ and $\gamma = \pm 60^\circ$), Eq. 3.94 yields $S_j^2 = 0.33$.

3.8.2 Skrynnikov modification to the Lipari-Szabo model

For interpretation of the methyl dynamics, we can assume that the fast local motion consists predominantly of a fast methyl spinning and fast side-chain motions (torsional librations, bond angle fluctuations, fast rotameric transitions). All these processes are described by a single local correlation time τ_e and a generalized order parameter S^2. If we assume the ideal tetrahedral geometry of the methyl group, the order parameter can be decomposed as $S^2 = 1/9 S^2_{axis}$, where the factor 1/9 originates from the fast methyl spinning and S^2_{axis} reflects the rapid fluctuation of the methyl averaging axis. The Lipari-Szabo spectral density then attains the form proposed by Skrynnikov [60]

$$J_{Skr}(\omega) = \frac{2}{5}\left[\frac{1}{9}S^2_{axis}\frac{\tau_m}{1+\omega^2\tau_m^2} + \left(1-\frac{1}{9}S^2_{axis}\right)\frac{(1-S^2)\tau}{1+\omega^2\tau^2}\right] \tag{3.95}$$

$$\tau^{-1} = \tau_m^{-1} + \tau_e^{-1}. \tag{3.96}$$

3.8.3 Extended Lipari-Szabo model by Clore

When dealing with a more complicated dynamics, it is sometimes necessary to account for the local motions at two different scales. Clore and coworkers [61; 62] introduced an extension of the Lipari-Szabo model by adding a local motion on a slow timescale, characterized by a slow local correlation time τ_s and generalized order parameter S^2_s, which is assumed to be independent on the fast local motion (τ_f, S^2_f) as well as the global reorientation (τ_M). The corresponding spectral density becomes

$$J_{Clore}(\omega) = \frac{2}{5}\left[\frac{S^2\tau_M}{1+\omega^2\tau_M^2} + \frac{(1-S^2_f)\tau_F}{1+\omega^2\tau_F^2} + \frac{(S^2_f-S^2)\tau_S}{1+\omega^2\tau_S^2}\right] \tag{3.97}$$

$$\tau_F^{-1} = \tau_M^{-1} + \tau_f^{-1} \tag{3.98}$$

$$\tau_S^{-1} = \tau_M^{-1} + \tau_s^{-1}. \tag{3.99}$$

If the faster motion can be assumed to be axially symmetric and independent of the slower motion, the global generalized order parameter can be decomposed as $S^2 = S^2_f S^2_s$.

3.8.4 Other models

Lipari-Szabo model and its modification are proven to be useful when interpreting dynamics of various types of flexible systems, ranging from small

molecules to large proteins. In some special cases, however, we might find the assumption about the uncorrelated global and local motion limiting. The situation arises mostly when internal molecular motions occur on a timescale similar to the global reorientation. In order to cover the coupling between the two motions, several approaches have been developed. Among them is, for example, the *slowly relaxing local structure* (SRLS) model developed by Polimeno and Freed [63; 64], and the *diffusive chain model* (DCM), discussed in Paper III.

3.9 Relaxation and chemical exchange

Even if the chemical exchange is slow on ^{1}H and ^{13}C chemical shift scale, it can still be comparable with the time scale of NMR relaxation and thus can affect significantly the apparent relaxation rates of species undergoing the exchange. In the presence of exchange, the Bloch-McConnell [65] equations (in the notation of Section 3.4.1) can be used to describe the relaxation of the longitudinal nuclear spin magnetizations of the free (I_F) and the bound (I_B) species

$$\frac{\mathrm{d}}{\mathrm{d}t}\begin{bmatrix} I_F \\ I_B \end{bmatrix} = \begin{bmatrix} -R_F - k_{FB} & k_{BF} \\ k_{FB} & -R_B - k_{BF} \end{bmatrix}\begin{bmatrix} I_F \\ I_B \end{bmatrix} + \\ + \begin{bmatrix} R_F & 0 \\ 0 & R_B \end{bmatrix}\begin{bmatrix} \mathrm{NOE}_F {I_F}^{eq} \\ \mathrm{NOE}_B {I_B}^{eq} \end{bmatrix}, \tag{3.100}$$

where R_F and R_B are the longitudinal relaxation rates of the free and the bound state, respectively, $\mathrm{NOE}_F {I_F}^{eq}$ and $\mathrm{NOE}_B {I_B}^{eq}$ are NOE-enhanced carbon-13 intensities at the steady-state in the presence of proton saturation, as they would be in case of no chemical exchange, and ${I_F}^{eq}$ and ${I_B}^{eq}$ denote the equilibrium magnetizations of the free and bound site.

When the exchange is present, the magnetizations at $t \to \infty$ (denoted as ${I_F}^{\infty}$ and ${I_B}^{\infty}$) can be obtained as a limit of the Bloch-McConnell equations 3.100. The NOE factors for the two states (NOE_F and NOE_B) can be determined according to

$$\mathrm{NOE}_F = (1+\eta_F) = \frac{k_{FB}{I_F}^{\infty} - k_{BF}{I_B}^{\infty}}{R_F {I_F}^{eq}} + \frac{{I_F}^{\infty}}{{I_F}^{eq}} \tag{3.101}$$

$$\mathrm{NOE}_B = (1+\eta_B) = \frac{k_{BF}{I_B}^{\infty} - k_{FB}{I_F}^{\infty}}{R_B {I_B}^{eq}} + \frac{{I_B}^{\infty}}{{I_B}^{eq}}. \tag{3.102}$$

The last terms in Eqs 3.101 and 3.102 are the standard steady-stare NOE enhancement factors and the first terms account for the chemical exchange.

4. Discussion of the papers

4.1 Host-guest complexes of Cryptophane-C

The remarkable ability of the cryptophanes to encapsulate a small organic guest inside their hydrophobic cavity is a rich and interesting research topic. Among the properties of interest of the host-guest complexes are the kinetics and thermodynamics of the complex formation and the dynamics of the guest inside the cavity. NMR, appropriately complemented by the quantum chemical calculations, is a technique that can provide insight into these systems. In our laboratory, cryptophanes and their complexes were extensively studied over the last decade [66–72]. Recently, a series of detailed studies, among others including Paper I and II, have significantly contributed to the understanding of the host-guest chemistry of cryptophanes. These studies have been also summarized in the doctoral thesis of Zoltan Takacs [73].

The exploration of the relation between the symmetry of the guest and the host molecule and the consequences for other molecular properties was studied in the work of Nikkhou Aski *et al.* [71]. In Paper I, we continued in this manner and investigated the cryptophane-C that has idealized C3 symmetry – the symmetry plane perpendicular to the three-fold symmetry axis is missing. This asymmetry raised a question whether there is a favorable orientation of the guest inside the cavity of the cryptophane. It seems reasonable to assume that the three-fold symmetry axes of cryptophane-C and the chloroform coincide. However, there is a possibility that the chloroform will be preferentially aligned with its C-H bond pointing either towards the methoxylated cap or towards the one that does not carry the methoxy substituents on the phenyl rings.

The integration of the intermolecular cross-peaks in the two-dimensional NOESY and ROESY experiments and the selective 1D NOESY and ROESY build-up measurements suggested the latter orientation to be the more probable one.

To the contrary, quantum chemical calculations of the complexed cryptophane showed lower energy for the former orientation. This was mostly because we underestimated the importance of sampling a sufficiently large part of the conformational space of cryptophane-C when performing the calculations.

Moreover, as it was discovered later, the geometry optimization performed in the calculations was not fully converged.

4.1.1 Cryptophane-C revisited

The contradictory results and the unclear conclusions of Paper I have proven that the conformational equilibria of the free and bound cryptophanes and their role played upon the complexation were not fully understood. The light on this problem was shed during the investigation of the cryptophane-D and its complexes [72]. Detailed investigation of samples of different concentration of the guest along with pure host provided improved understanding of the complexity of the encapsulation phenomenon. This was a motivation to reevaluate the cryptophane-C as a host.

In the same manner, a much more careful investigation of the cryptophane-C inclusion complexes was executed in Paper II. Both $CHCl_3$ and CH_2Cl_2 were included as guests, the NMR experiments were extended to include ^{1}H as well as ^{13}C measurements. Much more extensive DFT calculations, sampling larger part of the cryptophane-C conformational space, were performed.

We started the study with the free host investigation. The variable temperature measurements show broadening and splitting of the host resonances in both ^{1}H and ^{13}C spectra at low temperatures, giving an evidence of chemical (conformational) exchange present. We also observed differences in the spectra of the cryptophane-C after the chloroform and dichloromethane encapsulation. The plausible explanation is that the encapsulation of the guest can affect the conformational equilibria of the host, or possibly also hinder the host exchange.

The dichloromethane was in fast exchange between the bound and the free state throughout the whole temperature range, thus the kinetics of the system was studied by lineshape fitting [37; 38]. On the other hand, chloroform was in slow exchange at lower temperatures and its exchange rates were extracted using selective 1D NOESY experiments (see Section 3.4.2).

The determination of the association constant showed higher affinity of the cryptophane-C to dichloromethane than to chloroform. Another difference between the two guests is their mobility inside the cavity, explained by their different sizes [67–71]. The anticipated restricted motion of the larger chloroform molecule was confirmed by a relaxation study on carbon-13 labeled chloroform and subsequent Lipari-Szabo analysis.

The most important result from the study in Paper I was that one of the orientations of the encapsulated chloroform is significantly more probable than the other one. This conclusion, based on the NOESY and ROESY experiments, was fully confirmed in Paper II by the careful study of cross-relaxation

rates between the guest and the host protons. The cross-relaxation study was extended to the investigation of the linker conformations through the dipolar interaction between the host protons themselves.

In analogy to the cryptophane-D investigation, we performed DFT calculations for the free host, as well as for the host containing the chloroform guest in either of the possible orientations. This time, unlike in Paper I, the results of the calculations corroborated the experimental findings of the NOESY and ROESY experiments about the preferred orientation of the chloroform guest. Thus, it could be concluded that the the chloroform is more likely oriented with the C-H bond pointing towards the cap of cryptophane-C without the methoxy substituents.

Paper II provides therefore a very detailed picture of interaction and dynamics of the studied inclusion systems of cryptophane-C with chloroform and dichloromethane. After correcting the errors in the previous work, the NMR results are now consistent with the information obtained by quantum chemical calculations.

4.2 An integrated approach to interpretation of a complex dynamics in linear oligosaccharides

The description of molecules with internal dynamics is a challenging task that has led to the development of many approaches for interpreting NMR spin relaxation in flexible molecules over the past decades. Among the most extensively used is the Lipari-Szabo model-free formalism and its modifications (see Section 3.8), which are based on the assumption of the statistical independence of the global and local motion. This assumption may not be valid if the timescale separation between the rates of the two motions is small. This situation commonly arises for instance in oligosaccharides in the context of certain internal motions, where the mode-decoupling models fail to interpret the internal dynamic correctly [7]. Besides, multicomponent fitting procedure is usually required to access the model parameters, with all the problems related to fitting, i.e. the number of the experimental data close to the number of fitting parameters, or the existence of multiple minima in the χ^2 multidimensional surface.

A more advanced approach, the slowly relaxing local structure (SRLS) model, was developed by Polimeno and Freed [63; 64] and has been extensively applied to NMR studies of the local dynamics in proteins [74–78]. In SRLS, the relevant dynamics of the molecule is associated with two rigid rotors reorienting in a medium, coupled by a potential of mean torque. This means that SRLS exactly accounts for coupling of the motions if necessary and local

geometries (tilt angles between the different magnetic interactions) are a part of the set of the parameters used in the model definition. However, SRLS is of a phenomenological nature and provides empirical parameters rather than physical quantities calculated from the first principles. Furthermore, in the more complicated cases the fitting is sometimes unavoidable.

More recently, an integrated approach have been developed by the research group of professor Polimeno for calculation of both electron spin resonance [79; 80] and nuclear magnetic resonance [7; 81] spectroscopic observables of flexible molecules. The general protocol combines hydrodynamics-based evaluation of the dissipative properties, molecular dynamics (MD) or molecular mechanics (MM) for derivation of the local potential surfaces and a two-body stochastic approach for treating the coupled local and global dynamics. In a study preceding Paper III [82], a modification of this approach to account for a specific dynamics of γ-cyclodextrin was used to interpret the NMR relaxation data of the hydroxymethyl groups.

4.2.1 The diffusive chain model

In Paper III, a generalization of the approach described above, adapted to interpretation of NMR relaxation data, was proposed. The approach, called the *diffusive chain model* (DCM), considers explicitly the reorientation dynamics of the molecule represented as a flexible body consisting of rigid units connected with bonds, around which torsional motion is possible. The rigid units can be different in terms of shape, size and chemical composition. The schematic representation of the model is provided in Figure 4.1. This model was successfully used to predict the NMR relaxation data for a trisaccharide and a pentasaccharide (denoted LNF-1).

The first step in the DCM modeling is to select the set of N_T relevant torsions $\boldsymbol{\theta}$. For the trisaccharide molecule, two important torsion angles ω = O5–C5–C6–O6 and ψ_2 = C1″–O2′–C2′–H2′ (depicted in Figure 2.3) were chosen. The selection was based on the previous evidence from a similar disaccharide [7], on the J-coupling constant analysis [83], and it was further supported by the analysis of the trajectories of a 300 ns MD simulation.

The next step is to evaluate the diffusion tensor and the potential of the mean force (POMF). The method for the calculation of the diffusion tensor is based on the hydrodynamic approach. In our work, we employed the software DITE [84], which takes into account the internal flexibility of the molecule. The relevant part or the diffusion tensor (after projecting out the translational term) is partitioned into the purely rotational (RR), purely internal (II) and coupled roto-internal (RI) terms.

The full diffusion tensor depends on the molecular geometry, i.e. on the

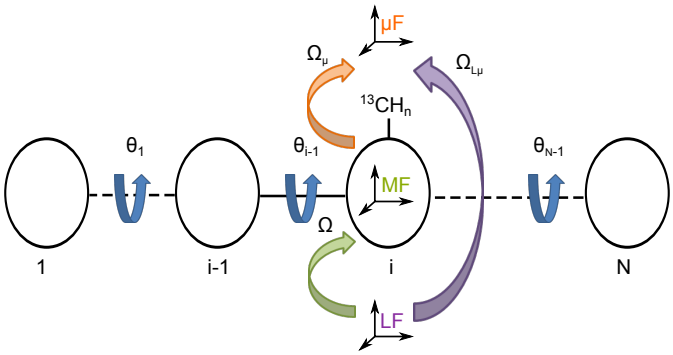

Figure 4.1: Schematic representation of the diffusive chain model (DCM). LF is the laboratory frame; MF is the molecular frame that diagonalizes the rotational part of the diffusion tensor placed on the reference body (*i* in the figure), which bears the spin probe; μF (μF = D1, D2 - dipolar frames) is the frame where the $\mu F^m athrmth$ magnetic tensor is diagonal. Euler angles transforming among frames are defined. Transformations from LF to any other frame are time dependent; transformations among the other frames are time independent.

set of variables $\boldsymbol{\theta}$. This dependence is often rather weak, especially for small molecules. Thus, for the trisaccharide, we assumed a configuration-independent diffusion tensor, calculated in the absolute energy minimum geometry with respect to ω and ψ_2, while for the larger system LNF-1, the $\boldsymbol{\theta}$-dependence of diffusion tensor was retained. Good agreement of the calculated data with the experimental NMR data justified this apparently strong approximation.

The second ingredient required is the potential of the mean force. We consider that, in isotropic systems, the POMF does not depend on the global reorientation of the molecule, but only on the internal torsions $\boldsymbol{\theta}$. An estimate of the equilibrium probability distribution of $\boldsymbol{\theta}$ can be obtained via the unbiased (applied for trisaccharide) or biased (applied for LNF-1) MD simulations trajectories, depending on the complexity of the system under study. The analytical expression for the potential surface is then derived.

Both the diffusion tensor and the POMF is then inserted into the diffusive operator of the Smoluchowski equation, which is then solved to calculate the required observables. One has the possibility to calculate the NMR relaxation parameters, in principle, without the need of multicomponent fitting. For our systems, the NMR relaxation data were calculated directly from the spectral densities making use of the Eqs. 3.71–3.73 for the conventional relaxation parameters and 3.88 for the cross-correlated rates. Relaxation parameters were calculated for the aliphatic $^{13}CH_n$ probes, therefore the CSA contributions could be neglected. In the case of the trisaccharide, spectral

densities were directly evaluated from the matrix elements of the diffusive operator. The number of the relevant degrees of freedom is significantly larger in LNF-1, therefore the spectral densities were evaluated using the standard Brownian dynamics approach in this case.

4.2.2 Performance of DCM model for the interpretation of NMR relaxations

An extensive set of NMR relaxation data, including both conventional parameters (T_1, T_2, NOE) and cross-correlated relaxation rates, was measured for both the trisaccharide and the pentasaccharide. NMR experiments for the trisaccharide were performed on the carbon-13 probe, placed on C6 carbon in the CH_2 group, (see Figure 2.3) at 298 K at three magnetic fields (500, 600 and 700 MHz). The relaxation data of the trisaccharide were simulated employing the DCM model with two fitted parameters, namely a multiplicative constant for the diffusion tensor and the H-C-H angle. The calculated data are in a good agreement with the experiment. The scaling constant for the diffusion tensor was 0.6, which is a reasonable correction considering both possible experimental deviations of temperature or viscosity and uncertainties of the adjustable parameters in the hydrodynamic simulations. The H-C-H angle of 116.3° shows a 6 % deviation from the tetrahedral value of 109.5° which is consitent with the observation in other similar systems [7; 58; 59] and indicates the effect of the internal motion, as shown in the previous paper [82]. The LNF-1 relaxation data were, on the other hand, simulated without fitting.

The diffusive chain model presented in Paper III provides a general framework to describe the dynamics of flexible molecules with internal degrees of freedom of torsional nature, where the coupling of the global and local motion can be expected. The model can provide a quantitatively adequate agreement of simulated relaxation data with the experimental ones at a relatively modest computational cost. Although the model is in principle applicable to biomolecules, for instance to small and medium oligosaccharides, as it was demonstrated in Paper III, it is clear that this approach is not yet applicable to large systems such as DNA, large proteins or polysaccharides due to the computational cost, rising with the increasing number of internal degrees of freedom.

What is not always straightforward is the selection of the relevant internal torsions. One has to use some chemical intuition, or, as in our case, rely on the data previously acquired on similar systems and theoretical calculations. On the other hand, the strength of the model lies in the possibility of calculation all the molecular parameters *a priori*, in the favorable cases without the use of the fitting parameters.

4.3 Complex dynamics of the *E. coli* O91 O-antigenic polysaccharide

Polysaccharides are important compounds in living organisms, possessing various functions. Capsular or loosely associated polysaccharides are found on the surface of both Gram-positive and Gram-negative bacteria. In the latter type, lipopolysaccharides (LPS) are an integral part of the outer membrane and their O-antigenic part is specific for each bacterial strain. The dynamics of the O-antigens is of significant importance in the general description of polysaccharides which are surrounding bacterial cell surfaces and in the presentation of antigenic epitopes to the immune system of an invaded host.

The *Escherichia coli* O91 O-antigenic polysaccharide was subject of a carbon-13 NMR relaxation study discussed in Paper IV. The identical O-antigenic polysaccharide with different carbon-13 labeling was previously studied by Lycknert and Widmalm [13]. The isotopic labels localized on the C1 carbons participating in the glycosidic linkages facilitated the determination of the internal dynamics of the polysaccharide chain. The O-antigen in our study received the isotopic labeling from the [6-^{13}C]glucose growth, which led to the labels on the exocyclic hydroxymethyl groups ($^{13}CH_2OH$) of the residues **D**, **A** and **C** and the methyl group ($^{13}CH_3$) of residue **E**. Both labeling schemes are depited in Figure 2.5.

The expectation was that our NMR relaxation study would reveal the conformational dynamics of the hydroxymethyls and presumably a fast dynamics of the methyl group, both possibly superimposed on the previously determined dynamics of the polymer chain.

The dynamics of the exocyclic groups was expected to be influenced also by the different configuration of the pyranosyl rings. The residues **C** and **D** are of the D-*gluco*-configuration (the C4-O4 bond is equatorial), whereas the residue **A** is in the D-*galacto*-configuration (the C4-O4 bond is axial), as depicted in Figure 4.2. For the D-*gluco*-configuration, the conformational equilibrium between the *gauche-gauche* and the *gauche-trans* conformation of the ω torsion angle is approximately 1:1 [7; 83; 85]. For the D-*galacto*-configuration, the equilibrium ratio between the *gauche-trans* and the *trans-gauche* conformation of ω is approximately 2:1 [83].

4.3.1 NMR experiments

The carbon-13 NMR spectrum of the polysaccharide shows signals from the CH_2OH groups of the residues **A**, **C** and **D** and the CH_3 group of residue **E**. In the work of Lycknert and Widmalm [13] on the [1-^{13}C] labeled material, a minor resonances close to the signals of the **E** residue was assigned to the

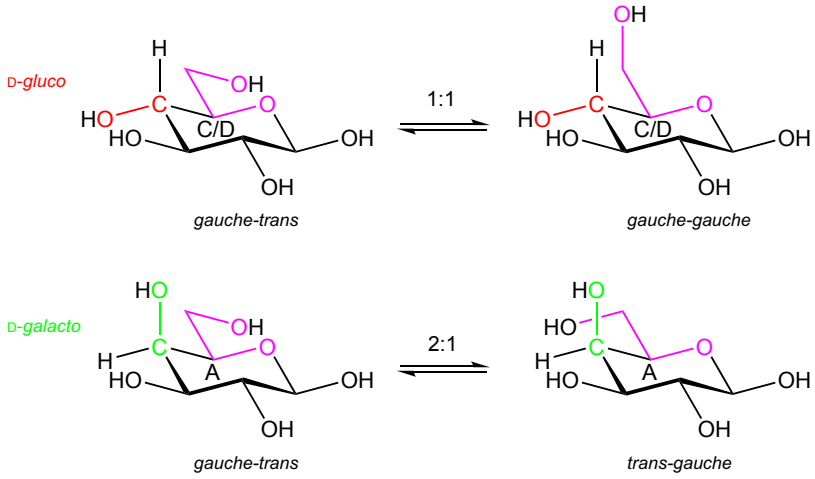

Figure 4.2: Configurations of the ω torsions for the D-hexopyranose sugars. The residues **C** and **D** have the D-*gluco* configuration, the residue **A** has the D-*galacto* configuration.

same residue of the terminal repeating unit, denoted **E**', reflecting the different chemical environment between the terminal and inner parts of the polysaccharide. In the spectra of the [6-^{13}C] labeled polysaccharide, besides the **E**', we observed also the resonance close to the **A** residue signal, which was consequently assigned to **A** residues of the terminal repeating unit, denoted **A**'.

NMR relaxation experiments were performed at magnetic fields of 16.4 and 21.1 T. The use of lower magnetic fields is not favorable due to the partial spectral overlap of the resonances of **A** and **D** residues, however, the resonances of **A** and **A**' residues were not well resolved even at the high magnetic fields used in this study. The terminal parts of the polysaccharide, which the **A**' signal originates from, clearly possess different dynamics than the rest of the polysaccharide. Nevertheless, we assume that the contribution of the **A**' resonance to the approximately ten-times more intense **A** resonance would be negligible.

When investigating the CH_2OH or CH_3 entities, it is important to take into consideration the effect of the cross-correlation (described in Section 3.7). This effect can cause deviation from the mono-exponential behavior of the T_1 and T_2 relaxation, thus the data obtained by the single exponential fitting may be biased. As discussed in Paper IV, the main problem arises in the case of spin-spin relaxation rates, where the cross-correlation effects between the dipolar interactions of the two protons are not easily suppressed by the experimental technique. Therefore, we had to employ the initial rate approach

recommended by Kay and Torchia [86], where only few initial intensities are used in the fitting procedure and which, unfortunately, leads to increased error of the T_2 data.

4.3.2 Interpretation of the dynamics

The interpretation of the NMR relaxation rates was a challenging task, owing to the very complex dynamics of the polysaccharide and rather sparse experimental data. Nevertheless, we already had some information about the motions in the polysaccharide from the analysis of the C1-labeled version. To decrease the number of fitted parameters, we used a fixed value of the global correlation time $\tau_M = 5.42$ ns as determined in the work of Lycknert and Widmalm [13].

Starting from the standard Lipari-Szabo model (Eq. 3.92–3.93), we found that it describes the dynamics of the **E** and **C** residues quite well. For the residues **A** and **D**, improvement was found when we moved to the extended Lipari-Szabo approach (Eq. 3.97–3.99).

For the hydroxymethyl groups, we expected that the conformational dynamics could be described by the two-site jump model. We evaluated the jump model parameters from the Lipari-Szabo generalized order parameter (Eq. 3.94) and fitted the data to the conformational jump model with the dipolar constant scaling as in the work of Ghalebani *et al.* [58]. The results were not clear-cut, nevertheless, we concluded that the exocyclic CH_2OH groups in residues **C** and **D** were undergoing the two-site jump with slightly distorted geometries compared to the ideal case. In the residue **A**, on the other hand, the rotational barrier was probably too low and the motion of the CH_2OH group was concluded to be a weakly restricted rotation.

It is important to point out that although moving from the simple Lipari-Szabo to the extended version of the model shows noticeable improvement of the quality of the fit, this might be ascribed to the larger number of parameters of the model. The three-exponential correlation function is likely to reproduce well almost any NMR experimental data (especially if they are few), one should thus be cautious when interpreting the results. In our case, the improvement was obvious for residues **A** and **D**. For the motion of the hydroxymethyls, the suggested physical picture, accounting for two local motions, can be viewed as the conformational changes (slow local motion) accompanied by the highly restricted motion in the potential energy minima (fast local motion). This was further supported by the results of the above mentioned two-site jump model analysis.

The resulting parameters of the model-free motional analysis, together with the data from the work of Lycknert and Widmalm [13] for comparison, are presented in Table 4.1. Here, only the models that were concluded to in-

terpret the motion of the particular residue most accurately are presented. The full analysis of our data, including errors, can be found in Paper IV.

The dynamics determined from the analysis of the C6 carbons is different than the one obtained for the C1 carbons, although some common trends can be observed. Clearly, the Lipari-Szabo order parameters of the hydroxymethyl groups (C6) are lower than the corresponding values for the C1 carbons. This might indicate an additional motion (i.e. the conformational changes) influencing the relaxation of the C6 sites. To draw a conclusion from the correlation times is more difficult. However, a trend is observed with a varying effective local correlation time as a function of the sugar residue, where the neighboring residues have local correlation times close to each others.

The relaxation study on the C6-labeled O-antigen revealed additional conformational dynamics in the polymer, one may thus visualize the polysaccharide as "beads on a string" with flexible attachments to the beads.

Table 4.1: Comparison of the model-free motional parameters of residues **A–E** as obtained for the [6-^{13}C] and [1-^{13}C] labeled O-antigen. LS stands for Lipari-Szabo model, ext. LS denotes the extended Lipari-Szabo model, LS + ex. means Lipari-Szabo with the exchange term R_{ex}.

E	**A**	**D**	**B**	**C**
		[6-^{13}C] labels		
LS	ext. LS	ext. LS		LS
$S^2 = 0.12$	$S^2 = 0.22$	$S^2 = 0.37$		$S^2 = 0.52$
	$S_f^2 = 0.84$	$S_f^2 = 0.84$		
	$S_s^2 = 0.26$	$S_s^2 = 0.44$		
	$\tau_s = 381$ ps	$\tau_s = 555$ ps		$\tau_e = 413$ ps
$\tau_e = 33.5$ ps	$\tau_f = 15$ ps			
		[1-^{13}C] labels		
E	**A**	**D**	**B**	**C**
LS	ext. LS	LS	LS	LS + ex.
$S^2 = 0.62$	$S^2 = 0.63$	$S^2 = 0.64$	$S^2 = 0.64$	$S^2 = 0.62$
$\tau_s = 517$ ps	$\tau_e = 387$ ps	$\tau_s = 366$ ps	$\tau_e = 376$ ps	$\tau_e = 455$ ps
				$R_{ex} = 2.7$ s^{-1}

4.4 Hydrogen-bonded molecular clusters of ethanol

Hydrogen bonding is a phenomenon that has been extensively studied in recent years and yet not all of its aspects are fully understood. The hydrogen-bonded structures in low-molecular-weight alcohols have been subjected to a vast number of studies employing infrared spectroscopy [87–90], X-ray or neutron diffraction [91–93], NMR spectroscopy [94], as well as theoretical approaches [20; 22; 95–99] and combinations of methods. A discussion of the findings of some of these works is presented in the introduction of Paper V.

Despite of the long-lasting interest in this subject, the details of the structure and dynamics of hydrogen-bonded species remain an open question. This fact was the motivation to open the issue of hydrogen bonding again and investigate the hydrogen-bonded clusters of ethanol.

Alcohols are among the simplest systems that undergo classical hydrogen-bonding. Compared to the complex three-dimensional hydrogen-bonded networks in water, alcohol clusters are known to have reduced dimensionality, preferring linear and cyclic topologies [100–103]. Therefore, ethanol provides a simple, yet realistic, model system which was a natural choice for our study.

Taking the advantage of the recent progress in NMR spectroscopy and computational techniques, we developed a novel method for investigation of the hydrogen bonding in liquid ethanol combining NMR diffusion experiments, hydrodynamic simulations and quantum chemical density functional theory (DFT) calculations. This method allowed us to report the average size of ethanol clusters in dilute solutions of ethanol throughout a wide range of temperatures.

We decided to investigate two samples of ethanol dissolved in deuterated hexane (concentrations 0.16 and 0.44 M) with an addition of TMS standard.

NMR diffusion measurements were quite straightforward method of choice, since the diffusion coefficient of ethanol clearly reflects the size of the hydrogen-bonded clusters in solution. It is important to mention that the clusters in liquid are not static structures. There is an evidence that reorganization of the hydrogen bonds occurs on a timescale of picoseconds or faster [89; 101; 102]. This fact is also reflected in the ^{1}H NMR spectrum, where a single peak of the OH groups is observed even at very low temperatures (approx. 180 K).

The reorganization of the clusters is therefore much faster than the diffusion mixing time Δ in NMR diffusion experiments (see Section 3.3), i.e. the hydrogen bonds are broken and reestablished many times during the period in which the diffusion is observed. This means that NMR diffusion measurements detect a population-weighted average of the diffusion coefficient of all clusters present.

However, transforming the diffusion properties into an actual number of

molecules (i.e. the size of the clusters) proved to be an arduous task.

The first problem was to transform the diffusion properties into the apparent hydrodynamic radius of the clusters since the viscosities of the deuterated hexane in our experimental temperature range are, to our best knowledge, not available in literature. We come back to this problem in Section 4.4.2.

The second difficulty was to obtain the size of an average cluster, assuming we know its diffusion coefficient. We decided to employ the hydrodynamic calculations, using the HydroNMR program [104], on the ethanol cluster structures previously calculated by the DFT method [105]. In this way it would be possible to associate the diffusion properties of the clusters obtained from experiments to those from the diffusion simulations and thus interpret the results quantitatively in terms of the size of the clusters.

4.4.1 TMS/hexane calibration experiments and simulations

Special attention was given to ensure that HydroNMR (designed for calculations on globular proteins) would give reliable results for small molecules as well. HydroNMR uses Stokes-Einstein approach that requires caution when used on systems where the size of the studied molecules is comparable to the size of the solvent molecules.

Tetramethylsilane (TMS) dissolved in hexane appeared to be a good choice of a "testing" system for the hydrodynamic simulations. Therefore, we prepared a calibration sample (TMS/hexane sample) containing 1 vol.% of TMS in non-deuterated hexane, whose viscosity is available in literature [106]. The idea was to perform both experiments and calculations on TMS, compare the results and possibly adjust input settings of the program. As an input of the HydroNMR program, the radius of the atomic spheres (AER) [107], that enters the bead model [108] used in the program for hydrodynamic calculations, can be specified. This parameter is of an empirical nature and we subjected it to optimization.

The measurements on the TMS/hexane sample turned out to be an experimental challenge. Because of the use of non-deuterated solvent, the sample was prepared in a coaxial tube with the outer tube containing deuterated methanol for the field-frequency lock. Thus the sensitivity was quite low, partly owing to the coaxial tube set, partly to the necessary low concentration of TMS and to the fact that TMS signal appeared close (approx. 1 ppm) to the much larger signal of hexane. Moreover, phase distortions, leading to baseline distortions, occurred during the processing. This problem was finally resolved by adding a spin-lock before acquisition into the diffusion pulse sequence (see Section 3.3).

Nevertheless, we found the optimized settings for the HydroNMR that

gave diffusion properties of TMS corresponding to experimental data, assuming that this would allow for correct simulations of the ethanol clusters.

Later on, we attempted to confirm the optimized settings for the program by the use of another system, hexamethylene tetramin (HMTA) dissolved in D_2O/DMSO solvent with three different compositions. This effort turned out to be unsuccessful, probably due to the hydration of HMTA, which appeared to have different hydrodynamic radius at different D_2O/DMSO ratios.

4.4.2 Viscosity determination

Before we turned to the hydrodynamic simulations of ethanol clusters, we had to deal with the problem of deuterated hexane viscosities. At this point, we utilized the measured diffusion coefficients of TMS in hexane again.

The viscosity of the deuterated hexane (with a low ethanol and TMS content) was obtained by assuming same hydrodynamic radius of TMS in both deuterated and non-deuterated hexane, employing the procedure described in detail in Paper V. The differences in the viscosity between the non-deuterated hexane and 0.16 M and 0.44 M ethanol samples containing deuterated hexane was found to be in average 4 % and 5 %, respectively.

We attempted to employ also other approaches to obtain the viscosity of the deuterated hexane. The capillary viscometer with a falling ball (Anton Paar) failed to provide reproducible results due to the too low viscosity. Moreover, it could not cover the whole temperature range of our experiments. Vibrating quartz fork method [109] seemed to be more promising but it would require further technical development.

4.4.3 Average size of molecular clusters of ethanol

Knowing the viscosities of the ethanol/hexane-d_{14} samples, we could obtain the hydrodynamic radii of the ethanol clusters from the experimental diffusion coefficients. Furthermore, we performed the hydrodynamic simulations on the DFT calculated structures of ethanol ranging from monomer to octamer, both linear and (for clusters larger than dimer) cyclic topologies. By comparing the results of the simulations with the experimental data, we were able to obtain the temperature dependent average size of the ethanol clusters at both concentrations (see Figure 4.3).

The hydrodynamic radius of ethanol obtained from the diffusion measurements generally decreases with increasing temperature. The more concentrated solution is composed of somewhat larger clusters in the whole investigated temperature range with average sizes, roughly, from dimer to heptamer.

At low temperatures (lower than approx. 210 K) the experimental hydrodynamic radii of both the 0.16 M and the 0.44 M ethanol samples reach a plateau

corresponding to clusters of average size of hexamer and heptamer, respectively. At the temperatures higher than 300 K, clusters of average size close to a dimer are present in the 0.44 M sample. In contrast, in the 0.16 M sample, the decrease stops at approx. 308 K, indicating that only monomers are significantly populated above this temperature. This experimental observation of a lower bound of hydrodynamic radius of ethanol is in excellent agreement with the calculated hydrodynamic radii. This fact strongly validates the employed methodology with the use of HydroNMR on small molecules with the prior calibration and reinforces our interpretation of the diffusion NMR data.

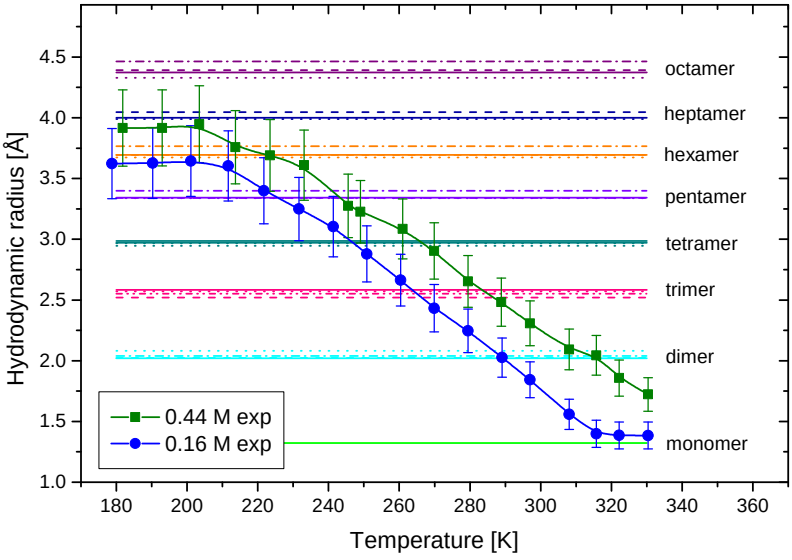

Figure 4.3: The average hydrodynamic radius of ethanol clusters from experiments and hydrodynamic simulations of the DFT-calculated cluster structures (horizontal lines).

Acknowledgements

I did not maybe find the answer to the ultimate question of life, the universe, and everything, but I'm quite sure there are many questions of mine that have been answered during my PhD. And this would not be possible without all the people I have met on my way.

I would like to thank my supervisors Jozef Kowalewski and Jan Lang for continuous support and help throughout whole period of my PhD. Without them, this would never come to a happy ending.

My thanks also belong to Zdeněk Němeček, dean of the Faculty of Mathematic and Physics at Charles University in Prague, and Stefan Nordlund, dean of the Faculty of Science at Stockholm University, who made the joint PhD project between the two universities possible.

I have spent a half of my entire PhD studies at the Department of Low Temperature Physics in Prague. I would like to thank especially the head of the department Ladislav Skrbek, the head of the Radiofrequency Spectroscopy division Helena Štěpánková and my colleagues Pavel Srb, Vašek Římal, Ríša Řezníček, Mikuláš Peksa, Kája Kouřil, Karel Bernášek, Vojta Chlan, Marián Grocký, and others for their scientific colaboration and help with problems of any imaginable kind.

The other half of my PhD have been spent with the people at the Department of Materials and Environmental Chemistry in Stockholm. I wish to thank the head of the department Gunnar Svensson, my coworkers Zoltan Takacs and Emilie Steiner for scientific help and fruitful discussions, and my colleagues and friends Guido Todde, Henrik Fahlquist, Samrad Shafeie, Ilich Ibarra, Daniel Eklöf, Alfredo Metere, Aleksander Jaworski, Jon Kapla, Amber Mace, Alexander Mirzoev, Claudia Turdean-Ionescu, Mikhail Voznesenskiy, and others for making my time in Stockholm enjoyable.

I would also like to thank Torbjörn Astlind, Rolf Eriksson, Ann-Britt Rönnell, and other members of the technical and administrative stuff for making the things run smoothly.

It would not be possible to run the NMR experiments if there weren't for the samples prepared at the Department of Organic Chemistry. I am especially thankful to Göran Widmalm, Olof Engström, and Robert Pendrill for providing unique samples, only of their kind on earth.

My thanks go also to the University of Padova in Italy, particularly to An-

tonino Polimeno, Mirco Zerbetto, and Dmytro Kotsyubynskyy for a fruitful scientific collaboration.

I also wish to thank my wonderful boyfriend Jožo and my family for all the love, support and understanding.

Last but not least, I wish to thank all my climbing, frisbee, and volleyball friends, who kept reminding me that there's more to life than just science.

So long, and thanks for all the fish!

References

[1] A. COLLET, J. GABARD, J. JACQUES, M. CESARIO, J. GUILHEM, AND C. PASCARD. **Synthesis and Absolute Configuration of Chiral (C_3) Cyclotriveratrylene Derivatives. Crystal structure of (M)-(–)-2,7,12-triethoxy-3,8,13-tris-[(R)-1-methoxycarbonylethoxy]-10,15-dihydro-5H-tribenzo[a,d,g]-cyclononene**. *J. Chem. Soc., Perkin Trans. 1*, pages 1630–1638, 1981. 4

[2] J. GABARD AND A. COLLET. **Synthesis of a (D_3)-Bis(cyclotriveratrylenyl) Macrocage by Stereospecific Replication of a (C_3)-Subunit**. *J. Chem. Soc., Chem. Commun.*, pages 1137–1139, 1981.

[3] J. CANCEILL, M. CESARIO, A. COLLET, J. GUILHEM, AND C. PASCARD. **A New Bis-Cyclotribenzyl Cavitand Capable of Selective Inclusion of Neutral Molecules in Solution. Crystal Structure of its CH_2Cl_2 Cavitate**. *J. Chem. Soc., Chem. Commun.*, pages 361–363, 1985.

[4] J. CANCEILL, M. CESARIO, A. COLLET, J. GUILHEM, C. RICHE, AND C. PASCARD. **Selective Recognition of Neutral Molecules: ^{1}H n.m.r. Study of the Complexation of CH_2Cl_2 and CH_2Br_2 by Cryptophane-D in Solution and Crystal Structure of its CH_2Cl_2 Cavitate**. *J. Chem. Soc., Chem. Commun.*, pages 339–341, 1986.

[5] CNCEILL AND A. COLLET. **Two-Step Synthesis of D_3 and C_{3h} Cryptophanes**. *J. Chem. Soc., Chem. Commun.*, pages 582–584, 1988. 4

[6] T. BROTIN AND J. P. DUTASTA. **Cryptophanes and Their Complexes - Present and Future**. *Chem. Rev.*, **109**:88–130, 2009. 4

[7] M. ZERBETTO, A. POLIMENO, D. KOTSYUBYNSKYY, L. GHALEBANI, J. KOWALEWSKI, E. MEIROVITCH, U. OLSSON, AND G. WIDMALM. **An Integrated Approach to NMR Spin Relaxation in Flexible Biomolecules: Application to β-D-glucopyranosyl-(1$\rightarrow$6)-α-D-mannopyranosyl-OMe**. *J. Chem. Phys.*, **131**:234501, 2009. 6, 41, 42, 44, 45

[8] R. STENUTZ, A. WEINTRAUB, AND G. WIDMALM. **The Structures of *Escherichia coli* O-Polysaccharide Antigens**. *FEMS Microbiol. Rev.*, **30**:382–403, 2006. 7

[9] J. YOTHER. **Capsules of *Streptococcus pneumoniae* and Other Bacteria: Paradigms for Polysaccharide Biosynthesis and Regulation**. *Annu. Rev. Microbiol.*, **65**:563–581, 2011. 8

[10] C. WHITFIELD. **Biosynthesis and Assembly of Capsular Polysaccharides in *Escherichia coli***. *Annu. Rev. Biochem.*, **75**:39–68, 2006.

[11] C. R. RAETZ AND C. WHITFIELD. **Lipopolysaccharide Endotoxins**. *Annu. Rev. Biochem.*, **71**:635–700, 2002. 8

[12] A. KJELLBERG, A. WEINTRAUB, AND G. WIDMALM. **Structural Determination and Biosynthesis Studies of O-Antigenic Polysaccharide from the Enterohemorrhagic *Escherichia coli* O91 Using ^{13}C-Enrichment and NMR Spectroscopy**. *Biochemistry*, **38**:12205–12211, 1999. 8

[13] K. LYCKNERT AND G. WIDMALM. **Dynamics of the *Escherichia coli* O91 O-Antigen Polysaccharide in Solution as Studied by Carbon-13 NMR Relaxation**. *Biomacromolecules*, **5**:1015–1020, 2004. 9, 45, 47

[14] T. STEINER. **The Hydrogen Bond in the Solid State**. *Angew. Chem. Int. Ed.*, **41**:48–76, 2002. 9

[15] I. ALKORTA, I. ROZAS, AND J. ELGUERO. **Non-Conventional Hydrogen Bonds**. *Chem. Soc. Rev.*, **27**:163–170, 1998.

[16] C. L. PERRIN AND J. B. NIELSON. **Strong Hydrogen Bonds in Chemistry and Biology**. *Annu. rev. Phys. Chem.*, **48**:511–544, 1997.

[17] B. KOJIĆ-PRODIĆ AND K. MOLCANOV. **The Nature of Hydrogen Bond: New Insights into Old Theories**. *Acta Chim. Slov.*, **55**:692–708, 2008. 9

[18] G. JEFFREY AND W. SAENGER. *Hydrogen Bonding in Biological Structures*. Springer, Berlin, 1991. 9

[19] G. JEFFREY. *An Introduction to Hydrogen Bonding*. Oxford University Press, 1997. 9

[20] L. SAIZ, J. A. PARDÓ, AND E. GUÀRDIA. **Dynamics and Hydrogen Bonding in Liquid Ethanol**. *Mol. Phys.*, **97**:897–905, 1999. 10, 49

[21] M. HÜLSEKOPF AND R. LUDWIG. **Temperature Dependence of Hydrogen Bonding in Alcohols**. *J. Mol. Liq.*, **85**:105–125, 2000.

[22] A. K. SUM AND S. I. SANDLER. **Ab Initio Calculations of Cooperativity Effects on Clusters of Methanol, Ethanol, 1-Propanol, and Methanethiol**. *J. Phys. Chem. A*, **104**:1121–1129, 2000. 10, 49

[23] U. LIDDEL AND N. F. RAMSEY. **Temperature Dependent Magnetic Shielding in Ethyl Alcohol**. *J. Chem. Phys.*, **19**:1608, 1951. 11

[24] J. T. ARNOLD AND M. E. PACKARD. **Variations in Absolute Chemical Shift of Nuclear Induction Signals of Hydroxyl Groups of Methyl and Ethyl Alcohol**. *J. Chem. Phys.*, **19**:1608, 1951. 11

[25] M. H. LEVITT. *Spin Dynamics: Basics of Nuclear Magnetic Resonance, Second Edition*. John Wiley & Sons, 2008. 12, 14

[26] J. KEELER. *Understanding NMR Spectroscopy*. John Wiley & Sons, 2010. 14

[27] J. KOWALEWSKI AND L. MÄLER. *Nuclear Spin Relaxation in Liquids: Theory, Experiments and Applications*. Taylor and Francis Group, 2006. 30, 31, 35

[28] A. ABRAGAM. *The Principles of Nuclear Magnetism*. Oxford University Press, 1961. 32

[29] C. P. SLICHTER. *Principles of Magnetic Resonance*. Springer Verlag, 1989. 12, 32

[30] F. BLOCH. **Nuclear Induction**. *Phys. Rev.*, **70**:460–467, 1946. 16

[31] A. EINSTEIN. **Über die von der molekularkinetischen Theorie der Wärme geforderte Bewegung von in ruhenden Flüssigkeiten suspendierten Teilchen**. *Analen der Physik*, **17**:549–560, 1905. 20

[32] E. STEJSKAL AND J. TANNER. **Spin Diffusion Measurements: Spin Echo in the Presence of a Time-Dependent Field Gradient**. *J. Phys. Chem.*, **42**(1):288–292, 1965. 20

[33] D. WU, A. CHEN, AND C. S. JOHNSON, JR. **An Improved Diffusion-Ordered Spectroscopy Incorporating Bipolar-Gradient Pulses**. *J. Magn. Reson.*, **117**:260–264, 1995. 21

[34] S. J. GIBBS AND C. S. JOHNSON, JR. **A PFG NMR Experiment for Accurate Diffusion and Flow Studies in the Presence of Eddy Currents**. *J. Magn. Reson.*, **93**:395–402, 1991. 21

[35] A. JERSCHOW AND R. MÜLLER. **Suppression of Convection Artifacts in Stimulated-Echo Diffusion Experiments. Double-Stimulated-Echo Experiments**. *J. Magn. Reson.*, **125**:372–375, 1997. 21

[36] M. PELTA, H. BARJAT, G. MORRIS, A. DAVIS, AND S. HAMMOND. **Pulse Sequences for High-Resolution Diffusion-Ordered Spectroscopy (HR-DOSY)**. *Magn. Reson. Chem.*, **36**:706–714, 1998. 21

[37] G. BINCH. **The Study of Intramolecular Rate Processes by Dynamic Nuclear Magnetic Resonance**. *Topics in Stereochemistry*, **3**:97–191, 1968. 23, 40

[38] V. ŘÍMAL, H. ŠTĚPÁNKOVÁ, AND J. ŠTĚPÁNEK. **Analysis of NMR Spectra in Case of Temperature-Dependent Chemical Exchange Between two Unequally Populated Sites**. *Concepts Magn. Reson. Part A*, **A38**:117–127, 2011. 23, 40

[39] K. STOTT, J. KEELER, Q. N. VAN, AND A. J. SHAKA. **One-Dimensional NOE Experiments Using Pulsed Field Gradients**. *Magn. Reson. Chem.*, **125**:302–324, 1997. 24

[40] S. MACURA, B. T. FARMER, AND L. R. BROWN. **An Improved Method for the Determination of Cross-Relaxation Rates from NOE Data**. *J. Magn. Reson.*, **70**:1969–1992, 1986. 24

[41] H. T. HU AND K. KRISHNAMURTHY. **Revisiting the Initial Rate Approximation in Kinetic NOE Measurements**. *J. Magn. Reson.*, **182**:173–177, 2006. 24

[42] I. SOLOMON. **Relaxation Processes in a System of Two Spins**. *Phys. Rev.*, **99**:559–565, 1955. 26

[43] J. KOWALEWSKI, M. EFFEMEY, AND J. JOKISAARI. **Dipole-Dipole Coupling Constant for a Directly Bonded CH Pair – A Carbon-13 Relaxation Study**. *J. Magn. Reson.*, **157**:171–177, 2002. 29

[44] E. HAHN. **Spin Echoes**. *Phys. Rev.*, **80**:580–595, 1950. 30

[45] H. CARR AND E. PURCELL. **Effect of Diffusion on Free Precession in Nuclear Magnetic Resonance Experiments**. *Phys. Rev.*, **94**:630–638, 1954. 31

[46] S. MEIBOOM AND D. GILL. **Modified Spin-Echo Method for Measuring Nuclear Relaxation Times**. *Rev. Sci. Instrum.*, **29**:688–691, 1958. 31

[47] A. G. PALMER, N. SKELTON, W. J. CHAZIN, P. E. WRIGHT, AND M. RANCE. **Suppression of the Effects of Cross-Correlation between Dipolar and Anisotropic Chemical Shift Relaxation Mechanisms in the Measurement of Spin-Spin Relaxation Rates**. *Mol. Phys.*, **75**:699–711, 1992. 31

[48] L. E. KAY, L. K. NICHOLSON, F. DELAGLIO, A. BAX, AND D. A. TORCHIA. **Pulse Sequences for Removal of the Effects of Cross Correlation between Dipolar and Chemical-Shift Anisotropy Relaxation Mechanisms on the Measurement of Heteronuclear T_1 and T_2 Values in Proteins**. *J. Magn. Reson.*, **97**:359–375, 1992. 31

[49] R. WANGSNESS AND F. BLOCH. **The Dynamic Theory of Nuclear Induction**. *Phys. Rev.*, **89**:728–739, 1953. 32

[50] A. REDFIELD. **The Theory of Relaxation Processes**. *Adv. Magn. Reson.*, **1**:1–32, 1965. 32

[51] A. KUMAR, R. C. R. GRACE, AND P. K. MADHU. **Cross-Correlation in NMR**. *Prog. Nucl. Magn. Reson. Spectr.*, **37**:191–319, 2000. 33

[52] L. G. WERBELOW AND D. M. GRANT. **Intramolecular Dipolar Relaxation in Multispin System**. *Adv. Magn. Reson.*, **9**:182–299, 1977. 34

[53] L. GHALEBANI, P. BERNATOWICZ, S. NIKKHOU ASKI, AND J. KOWALEWSKI. **Cross-Correlated and Conventional Dipolar Carbon-13 Relaxation in Methylene Groups in Small, Symmetric Molecules**. *Concepts Magn. Reson. Part A*, **30A**:100–115, 2007. 35

[54] V. A. DARAGAN AND K. H. MAYO. **Motional Model Analyses of Protein and Peptide Dynamics Using ^{13}C and ^{15}N NMR Relaxation**. *Prog. Nucl. Magn. Reson. Spectr.*, **31**:63–105, 1997. 36

[55] V. A. JARYMOWYCZ AND M. J. STONE. **Fast Time Scale Dynamics of Protein Backbones: NMR Relaxation Methods, Applications, and Functional Consequences**. *Chem. Rev.*, **106**:1624–1671, 2006. 36

[56] G. LIPARI AND A. SZABO. **Model-Free Approach to the Interpretation of Nuclear Magnetic Resonance Relaxation in Macromolecules. 1. Theory and Range of Validity**. *J. Am. Chem. Soc.*, **104**:4546–4559, 1982. 36

[57] G. LIPARI AND A. SZABO. **Model-Free Approach to the Interpretation of Nuclear Magnetic Resonance Relaxation in Macromolecules. 2. Analysis of Experimental Results**. *J. Am. Chem. Soc.*, **104**:4559–4570, 1982. 36

[58] L. GHALEBANI, D. KOTSYUBYNSKYY, AND J. KOWALEWSKI. **NMR Relaxation Interference Effects and Internal Dynamics in γ-Cyclodextrin**. *J. Magn. Reson.*, **195**:1–8, 2008. 36, 44, 47

[59] K. E. KÖVÉR, G. BATTA, J. KOWALEWSKI, L. GHALEBANI, AND D. KRUK. **Internal Dynamics of Hydroxymethyl Rotation from CH_2 Cross-Correlated Dipolar Relaxation in Methyl-β-D-Glucopyranoside**. *J. Magn. Reson.*, **167**:273–281, 2004. 36, 44

[60] N. R. SKRYNNIKOV, O. MILLET, AND L. E. KAY. **Deuterium Spin Probes of Side-Chain Dynamics in Proteins. 2. Spectral Density Mapping and Identification of Nanosecond Time-Scale Side-Chain Motions**. *J. Am. Chem. Soc.*, **124**:6449–6460, 2002. 37

[61] G. M. CLORE, A. SZABO, A. BAX, L. E. KAY, P. DRISCOLL, AND A. M. GRONENBORN. **Deviations from the Simple Two-Parameter Model-Free Approach to the Interpretation of Nitrogen-15 Nuclear Magnetic Relaxation of Proteins**. *J. Am. Chem. Soc.*, **112**:4989–4991, 1990. 37

[62] G. M. CLORE, P. C. DRISCOLL, P. T. WINGFIELD, AND A. M. GRONENBORN. **Analysis of the Backbone Dynamics of Interleukin-1β Using Two-Dimensional Inverse Detected Heteronuclear ^{15}N - ^{1}H NMR Spectroscopy**. *Biochem.*, **29**:7387–7401, 1990. 37

[63] A. POLIMENO AND J. H. FREED. **A Many-Body Stochastic Approach to Rotational Motions in Liquids**. *Adv. Chem. Phys.*, **83**:89–206, 1993. 38, 41

[64] A. POLIMENO AND J. H. FREED. **Slow Motional ESR in Complex Fluids: The Slowly Relaxing Local Structure Model of Solvent Cage Effects**. *J. Chem. Phys.*, **99**:10995, 1995. 38, 41

[65] H. M. MCCONNELL. **Reaction Rates By Nuclear Magnetic Resonance**. *J. Chem. Phys.*, **28**:430–431, 1958. 38

[66] J. LANG, J. J. DECHTER, M. EFFEMEY, AND J. KOWALEWSKI. **Dynamics of an Inclusion Complex of Chloroform and Cryptophane-E: Evidence for a Strongly Anisotropic van der Waals Bond**. *J. Am. Chem. Soc.*, **123**:7852–7858, 2001. 39

[67] Z. TOŠNER, J. LANG, D. SANDSTRÖM, O. PETROV, AND J. KOWALEWSKI. **Dynamics of an Inclusion Complex of Dichloromethane and Cryptophane-E**. *J. Phys. Chem. A*, **106**:8870–8875, 2002. 40

[68] Z. TOŠNER, O. PETROV, S. V. DVINSKIKH, J. KOWALEWSKI, AND D. SANDSTRÖM. **A ^{13}C Solid-State NMR Study of Cryptophane-E:Chloromethane Inclusion Complexes**. *Chem. Phys. Lett.*, **388**:208–211, 2004.

[69] O. PETROV, Z. TOŠNER, I. CSÖREGH, J. KOWALEWSKI, AND D. SANDSTRÖM. **Dynamics of Chloromethanes in Cryptophane-E Inclusion Complexes: A ^{2}H Solid-State NMR and X-ray Diffraction Study**. *J. Phys. Chem. A*, **109**:4442–4451, 2005.

[70] S. NIKKHOU ASKI, Z. TAKACS, AND J. KOWALEWSKI. **Inclusion Complexes of Cryptophane-E with Dichloromethane and Chloroform: A Thermodynamic and Kinetic Study Using the 1D-EXSY NMR Method**. *Magn. Reson. Chem.*, **46**:1135–1140, 2008.

[71] S. NIKKHOU ASKI, A. Y. H. LO, T. BROTIN, J. P. DUTASTA, M. EDÉN, AND J. KOWALEWSKI. **Studies of Inclusion Complexes of Dichloromethane in Cryptophanes by Exchange Kinetics and ^{13}C NMR in Solution and the Solid State**. *J. Phys. Chem. C*, **112**:13873–13881, 2008. 39, 40

[72] Z. TAKACS, T. BROTIN, J.-P. DUTASTA, J. LANG, G. TODDE, AND J. KOWALEWSKI. **Inclusion of Chloromethane Guests Affects Conformation and Internal Dynamics of Cryptophane-D Host**. *J. Phys. Chem. B*, **116**:7898–7913, 2012. 39, 40

[73] Z. TAKACS. *Chloromethane Complexation by Cryptophanes: Host-Guest Chemistry Investigated by NMR and Quantum Chemical Calculations*. doctoral thesis, Stockholm University, 2012. 39

[74] E. MEIROVITCH, Y. E. SHAPIRO, A. POLIMENO, AND J. H. FREED. **Protein Dynamics from NMR: The Slowly Relaxing Local Structure Analysis Compared with Model-Free Analysis**. *J. Phys. Chem. A*, **110**:8366–8396, 2006. 41

[75] E. MEIROVITCH, Y. E. SHAPIRO, A. POLIMENO, AND J. H. FREED. **Structural Dynamics of Bio-Macromolecules by NMR: The Slowly Relaxing Local Structure Approach**. *Prog. Nucl. Magn. Reson. Spectrosc.*, **56**:360–405, 2010.

[76] Y. E. SHAPIRO, A. POLIMENO, J. H. FREED, AND E. MEIROVITCH. **Methyl Dynamics of a Ca^{2+}-Calmodulin-Peptide Complex from NMR/SRLS**. *J. Phys. Chem. B*, **115**:354–365, 2011.

[77] E. MEIROVITCH, M. ZERBETTO, A. POLIMENO, AND J. H. FREED. **Backbone Dynamics of Deoxy and Carbonmonoxy Hemoglobin by NMR/SRLS**. *J. Phys. Chem. B*, **115**:143–157, 2011.

[78] E. MEIROVITCH, Y. E. SHAPIRO, M. ZERBETTO, AND A. POLIMENO. **SRLS Analysis of ^{15}N Spin Relaxation from *E. coli* Ribonuclease HI: The Tensorial Perspective**. *J. Phys. Chem. B*, **116**:886–894, 2012. 41

[79] V. BARONE AND A. POLIMENO. **Toward an Integrated Computational Approach to CW-ESR Spectra of Free Radicals**. *Phys. Chem. Chem. Phys.*, **8**:4609–4629, 2006. 42

[80] M. ZERBETTO, A. POLIMENO, AND V. BARONE. **Simulation of Electron Spin Resonance Spectroscopy in Diverse Environments: An Integrated Approach**. *Comput. Phys. Commun.*, **180**:2680–2697, 2009. 42

[81] M. ZERBETTO, M. BUCK, E. MEIROVITCH, AND A. POLIMENO. **Integrated Computational Approach to the Analysis of NMR Relaxation in Proteins: Application to ps-ns Main Chain ^{15}N-^{1}H and Global Dynamics of the Rho GTPase Binding Domain of Plexin-B1**. *J. Phys. Chem. B*, **115**:376–388, 2011. 42

[82] M. ZERBETTO, D. KOTSYUBYNSKYY, J. KOWALEWSKI, G. WIDMALM, AND A. POLIMENO. **Stochastic Modeling of Flexible Biomolecules Applied to NMR Relaxation. I. Internal Dynamics of Cyclodextrins: γ-Cyclodextrin as a Case Study**. *J. Phys. Chem. B*, **116**:13159–13171, 2012. 42, 44

[83] R. STENUTZ, I. CARMICHAEL, G. WIDMALM, AND A. S. SERIANNI. **Hydroxymethyl Group Conformation in Saccharides: Structural Dependencies of $^2J_{HH}$, $^3J_{HH}$, and $^1J_{CH}$ Spin-Spin Coupling Constants**. *J. Org. Chem.*, **67**:949–958, 2002. 42, 45

[84] V. BARONE, M. ZERBETTO, AND A. POLIMENO. **Hydrodynamic Modeling of Diffusion Tensor Properties of Flexible Molecules**. *J. Comput. Chem.*, **30**:2–12, 2009. 42

[85] U. OLSSON, E. SÄWÉN, R. STENUTZ, AND G. WIDMALM. **Conformation Flexibility and Dynamics of Two $(1 \rightarrow 6)$-Linked Disaccharides Related to an Oligosaccharide Epitope Expressed on Malignant Tumor Cells**. *Chem. Eur. J.*, **15**:8886–8894, 2009. 45

[86] L. E. KAY AND D. A. TORCHIA. **The Effects of Dipolar Cross Correlation on ^{13}C Methyl-Carbon T_1, T_2, and NOE Measurements in Macromolecules**. *J. Magn. Reson.*, **95**:536–547, 1991. 47

[87] H. GRAENER, T. Q. YE, AND A. LAUBEREAU. **Ultrafast Dynamics of Hydrogen Bonds Directly Observed by Time-Resolved Infrared Spectroscopy**. *J. Chem. Phys.*, **90**:3413, 1989. 49

[88] K. M. MURDOCH, T. D. FERRIS, J. C. WRIGHT, AND T. C. FARRAR. **Infrared Spectroscopy of Ethanol Clusters in Ethanol-Hexane Binary Solutions**. *J. Chem. Phys.*, **116**:5717, 2002.

[89] K. J. GAFFNEY, I. R. PILETIC, AND M. D. FAYER. **Orientational Relaxation and Vibrational Excitation Transfer in Methanol-Carbon Tetrachloride Solutions**. *J. Chem. Phys.*, **118**:2270, 2003. 49

[90] P. SASSI, F. PALOMBO, R. S. CATALIOTTI, M. PAOLANTONI, AND A. MORRESI. **Distribution of H-Bonding Aggregates in *tert*-Butyl Alcohol: The Pure Liquid and Its Alkane Mixtures**. *J. Phys. Chem. A*, **111**:6020–6027, 2007. 49

[91] S. SARKAR AND R. N. JOARDER. **Molecular Clusters and Correlations in Liquid Methanol at Room Temperature**. *J. Chem. Phys.*, **99**:2032, 1993. 49

[92] S. SARKAR AND R. N. JOARDER. **Molecular Clusters in Liquid Ethanol at Room Temperature**. *J. Chem. Phys.*, **100**:5118, 1994.

[93] T. YAMAGUCHI, K. HIDAKA, AND A. K. SOPER. **The Structure of Liquid Methanol Revisited: a Neutron Diffraction Experiment at $-80\,^{\circ}$C and $+25\,^{\circ}$C**. *Mol. Phys.*, **96**:1159–1168, 1999. 49

[94] T. D. FERRIS AND T. C. FARRAR. **The Temperature Dependence of the Deuterium Quadrupole Coupling Parameter and The Rotational Correlation Time of The OD Internuclear Vector in Neat Ethanol-d_1**. *Mol. Phys.*, **100**:303–309, 2002. 49

[95] V. DYCZMONS. **Dimers of Ethanol**. *J. Phys. Chem. A*, **108**:2080–2086, 2004. 49

[96] S. M. MEJÍA, J. F. ESPINAL, A. RESTREPO, AND F. MONDRAGÓN. **Molecular Interaction of (Ethanol)$_2$-Water Heterodimer**. *J. Phys. Chem. A*, **111**:8250–8256, 2010.

[97] S. M. MEJÍA, J. F. ESPINAL, AND F. MONDRAGÓN. **Cooperative Effects on The Structure and Stability of (Ethanol)$_3$-Water, (Methanol)$_3$-Water Heterotetramers and (Ethanol)$_4$, (Methanol)$_4$ Tetramers**. *J. Mol. Struct. THEOCHEM*, **901**:186–193, 2009.

[98] J. DAVID, D. GUERRA, AND A. RESTREPO. **Structural Characterization of the (Methanol)$_4$ Potential Energy Surface**. *J. Phys. Chem. A*, **113**:10167–10173, 2009.

[99] K. BLOCH AND C. P. LAWRENCE. **Hydrogen Bond Lifetimes and Clustering of Methanol in Carbon Tetrachloride Solutions**. *J. Phys. Chem. B*, **114**:293–297, 2010. 49

[100] C. P. BROCK AND L. L. DUNCAN. **Anomalous Space-Group Frequencies for Monoalcohols $\mathbf{C}_n\mathbf{H}_m\mathbf{OH}$**. *Chem. Mater.*, **6**:1307–1312, 1994. 49

[101] J. GAFFNEY, I. R. PILETIC, AND M. D. FAYER. **Hydrogen Bond Breaking and Reformation in Alcohol Oligomers Following Vibrational Relaxation of a Non-Hydrogen-Bond Donating Hydroxyl Stretch**. *J. Phys. Chem. A*, **106**:9428–9435, 2002. 49

[102] J. GAFFNEY, P. H. DAVIS, I. R. PILETIC, N. E. LEVINGER, AND M. D. FAYER. **Hydrogen Bond Dissociation and Reformation in Methanol Oligomers Following Hydroxyl Stretch Relaxation**. *J. Phys. Chem. A*, **106**:12012–12023, 2002. 49

[103] J. B. ASBURY, T. STEINEL, AND M. D. FAYER. **Hydrogen Bond Networks: Structure and Evolution after Hydrogen Bond Breaking**. *J. Phys. Chem. B*, **108**:6544–6554, 2004. 49

[104] J. G. DE LA TORRE, M. L. HUERTAS, AND B. CARRASCO. **HYDRONMR: Prediction of NMR Relaxation of Globular Proteins from Atomic-Level Structures and Hydrodynamic Calculations**. *J. Magn. Reson.*, **147**:138–46, 2000. 50

[105] L. BENDA. *Computational Study on Structure and Properties of Ethanol Clusters*. diploma thesis, Charles University in Prague, 2006. 50

[106] E. B. GILLER AND H. G. DRICKAMER. **Viscosity of Normal Paraffins near the Freezing Point**. *Ind. Eng. Chem. Res.*, **41**:2067, 1949. 50

[107] B. CARRASCO AND J. G. DE LA TORRE. **Hydrodynamic Properties of Rigid Particles: Comparison of Different Modeling and Computational Procedures**. *J. Biophys.*, **76**:3044–3057, 1999. 50

[108] V. A. BLOOMFIELD, W. O. DALTON, AND K. E. VAN HOLDE. **Frictional Coefficients of Multisubunit Structures. I. Theory**. *Biopolymers*, **5**:135–148, 1967. 50

[109] H. DIVIŠOVÁ, J. LANG, M. ROTTER, AND D. SCHMORANZER. **Measurement of Viscosity in Small Volumes of Fluids by Tuning Fork Oscillators**. *EPJ Web of Conferences*, **25**:01008, 2012. 51